A project funded by the United Nations Development Programme/Global Environment Facility (UNDP/GEF) and executed by the United Nations Office for Project Services (UNOPS)

Special Study on Sediment Discharge and Its Consequences (SedSS)

Technical Report Number 5

SOIL EROSION MODELLING IN THE LAKE TANGANYIKA CATCHMENT

by
N Drake, M Wooster, E Symeonakis
and X Zhang

1999

Pollution Control and Other Measures to Protect Biodiversity in Lake Tanganyika (RAF/92/G32)
Lutte contre la pollution et autres mesures visant à protéger la biodiversité du Lac Tanganyika (RAF/92/G32)

Le Projet sur la diversité biologique du lac Tanganyika a été formulé pour aider les quatre Etats riverains (Burundi, Congo, Tanzanie et Zambie) à élaborer un système efficace et durable pour gérer et conserver la diversité biologique du lac Tanganyika dans un avenir prévisible. Il est financé par le GEF (Fonds pour l'environnement mondial) par le biais du Programme des Nations Unies pour le développement (PNUD)"	The Lake Tanganyika Biodiversity Project has been formulated to help the four riparian states (Burundi, Congo, Tanzania and Zambia) produce an effective and sustainable system for managing and conserving the biodiversity of Lake Tanganyika into the foreseeable future. It is funded by the Global Environmental Facility through the United Nations Development Programme.

Burundi: Institut National pour Environnement et Conservation de la Nature
D R Congo: Ministrie Environnement et Conservation de la Nature
Tanzania: Vice President's Office, Division of Environment
Zambia: Environmental Council of Zambia

Enquiries about this publication, or requests for copies should be addressed to:

Project Field Co-ordinator
Lake Tanganyika Biodiversity Project
PO Box 5956
Dar es Salaam, Tanzania

UK Co-ordinator,
Lake Tanganyika Biodiversity Project
Natural Resources Institute
Central Avenue, Chatham, Kent, ME4 4TB, UK

Lake Tanganyika Biodiversity Project Special Study
on Sediment Discharge and its Consequences:

Soil Erosion Modelling in the Lake Tanganyika Catchment

By Nick Drake, Martin Wooster, Elias Symeonakis, and Xiaoyang Zhang
Department of Geography,
King's College London,
Strand, London WC2R 2LS.

Abstract

A regional scale soil erosion has been implemented on a daily and decadal timestep for the Lake Tanganyika catchment using remote sensing estimates of rainfall and vegetation cover. Remote sensing estimates of rainfall were found to be superior to those obtained using kriging of GTS raingauge data. Parameterisation of the model with these different spatial rainfall estimates produced quite different results in certain instances.

The model has been implemented in a number of different ways in order to derive different information about both the lake and its catchment. We have demonstrated how the model can be used in near real time monitoring, and have shown how retrospective studies can be parameterised using the FEWS archive of rainfall estimates and ARTEMIS NDVI archive. Furthermore, we have developed scenarios of land degradation and deforestation in order to determine how the catchment responds under these conditions. Finally, we have developed a method of sediment routing that calculates sediment delivery ratio in order to estimate the amount of eroded sediment that reaches the lake.

The results suggest that there are three regions of the lake catchment (one each in Burundi, Zaire and Tanzania) that are particularly sensitive to erosion. In Burundi deforestation is almost total and significant sediments appear to be entering the northern part of Lake Tanganyika. In Tanzania and The Democratic Republic of Congo deforestation is less complete and sediment yields do not appear to be so high.

1. Introduction

Lake Tanganyika is extremely large and extremely old. It contains around one sixth of the worlds liquid freshwater and is almost one and a half kilometres at its deepest point. The present three lake basins have been water-filled for at least ten million years and some sediments date back twice this period Patterson and Makin (1998). In addition to these almost unparalleled physical characteristics, the lake is also a truly unique ecosystem; the second most biologically diverse lake on Earth. There are at least 300 endemic fish species in the lake and more are continually being discovered. Six of these species occur in vast numbers and are an important source of food and income for the local population.

The aim of the Lake Tanganyika Biodiversity Project (LTBP) is to assist the four riparian states (Burundi, Democratic Republic of Congo, Tanzania and Zambia) produce an effective and sustainable system for managing and conserving the unique biodiversity of Lake Tanganyika into the foreseeable future. This effort involves a detailed scientific study of the lake and surrounding catchment, including a major investigation into sedimentation. One of the main aims of the Sedimentation Special Study is to assess the movement and impact of soil entering the lake, since previous work has indicated that sediment inputs from accelerating land erosion may be the main current environmental threat, far outweighing that from organic pollution (Vandelannoote *et al.*, 1996).

Cohen *et al.*, (1993) showed how the species richness of fish and ostracods was significantly reduced in regions of the lake subject to sedimentation from land erosion, with species richness in some cases being 65% lower. The vast majority of these species are endemic to the lake, or even to specific regions of the lake, and have highly particular habitat requirements that are likely to be severely impacted by increases in suspended sediment concentration brought about by erosion within the catchment and sediment transport into the lake. The LTBP sediment study is supporting the collection and analysis of a series of lake sediment cores, allowing a historical investigation into the relationship between previous land disturbances, sedimentation rates and lake biota diversity in order to confirm results gained from contemporary data.

With regard to the future development, conservation and resource utilisation strategy recommended by the LTBP, the importance of sediment pollution requires that the erosion of the entire lake drainage basin be investigated, ideally with a modelling approach that allows future scenarios to be tested and their impact on lake sedimentation rates assessed. The current study forms part of the development of this capability, which combines remote sensing data collection and analysis with spatial modelling of the erosion at the catchment scale and investigation into the transport of the eroded soil particles into Lake Tanganyika.

2. Aims and Objectives

A soil erosion model of the Lake Tanganyika catchment and the surrounding area has been implemented at the regional scale (1-8 km pixel size) on a daily to dekadal time step. The model predicts soil detachment by rainsplash and the ability of overland flow to transport this material. However, it does not consider where the sediment is transported to or any subsequent deposition.

The project aimed to achieve the following objectives:

1) Implement a retrospective study for the 1996 wet season in order to assess the feasibility of using the model for long term monitoring.

2) Determine the optimal methods for incorporating spatial estimates of rainfall into the soil erosion model, concentrating on a comparison of interpolated raingauge data and remote sensing derived rainfall estimates.

3) Investigate the routing of erosion (i.e. transport and deposition) in order to estimate actual sediment inputs to the lake.

4) Define areas within the catchment that are most sensitive to erosion by predicting likely increases in erosion rates based on scenarios of extreme rainfall events, land degradation and deforestation.

5) Develop a demonstrator for real-time erosion prediction using data from the LARST AVHRR receiving station, currently based in Kigoma, Tanzania.

3. The Soil Erosion Model Parameterisation

The soil erosion model used is that of Thornes (1985, 1989):

$$E = k\, OF^2\, s^{1.67} e^{-0.07v} \qquad (1)$$

where E is erosion, k is a soil erodibility coefficient, OF is overland flow, s is the slope of the land, and *v* the vegetation cover.

3.1 Model Parameterisation

The model (1) has been parameterised using remote sensing and GIS data as outlined below.

3.1.1Vegetation Cover

Vegetation cover is estimated from normalised difference vegetation index (NDVI) information, derived from NOAA AVHRR data. For the historical data we use dekadal ARTEMIS NDVI data (7.5 km spatial resolution), obtained from a published archive. For the real-time demonstrator we use local area coverage (LAC) AVHRR data (1 km spatial resolution), obtained from Kigoma, which we have calibrated, geocoded and converted into NDVI measurements using the NOAA Operations Manager (NOM) software developed by NRI. Numerous authors have found a relationship between either total or green vegetation cover (*v*) and NDVI and these data have been collated by Drake *et al.,* (1995) and Zhang *et al.,* (1999) (Figure 1). It is clear that the relationship between *v* and NDVI measured in the field using radiometers and spectroradiometers is shifted when compared to the relationship with NDVI obtained from AVHRR imagery. This is due to atmospheric effects that affect the satellite-based measurements but not the spectroradiometer data. Because of this, using the regression relationship between *v* and NDVI based on the whole collated dataset provides an underestimation of vegetation cover when using AVHRR-derived NDVI data. For estimating vegetation cover effectively, therefore, a new regression relationship was calculated using only the AVHRR derived NDVI and the vegetation cover information:

$$Vc = 1.333 + 131.877\,NDVI$$

Fit statistics: $r^2 = 0.73$, $F=241.63$, $p=4.26\text{x}10^{-27}$.

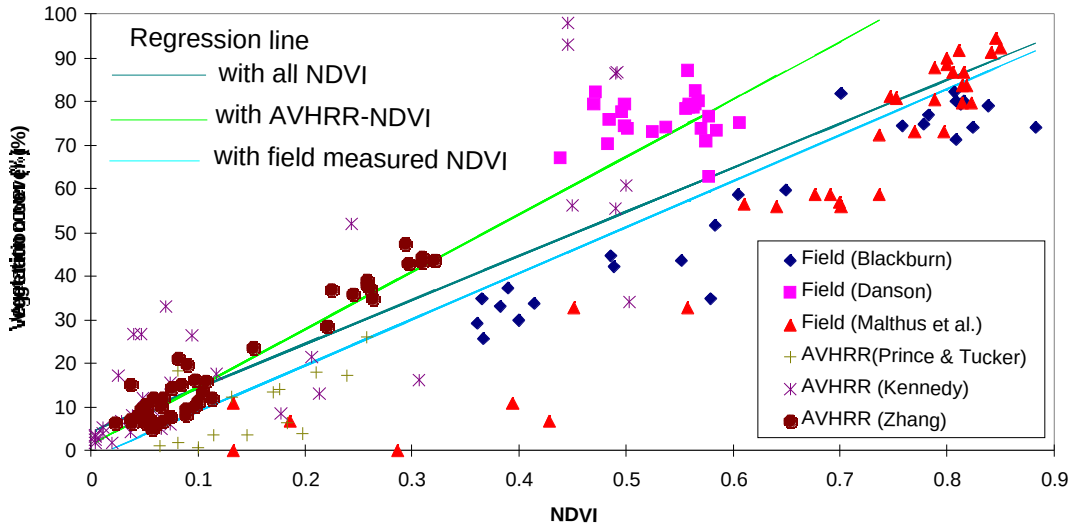

Figure 1. Scattergram showing the relationship between percent vegetation cover (*v*) and NDVI data found by previous researchers. NDVI data were calculated from ground-based spectroradiometer (field) or satellite-based (AVHRR) radiometric measurements.

One of the problems with AVHRR-derived NDVI imagery is that it contains missing data where there is cloud cover for the entire dekad (Figure 2, top and bottom left). We overcome this by filling the gaps with the average NDVI for that location from the preceding and following dekads (Figure 2, top and bottom right). If there are still gaps then this process of averaging is continued until they are filled. The data are then converted into vegetation cover using the calibration outlined above. Figure 3 shows that there are a few locations in Rwanda and Burundi where cloud cover exists for the entire month of March 1996. It is true that these regions will tend to suffer high overland flow and erosion because it is raining for much of the time. However, they are also the places where the actual vegetation cover is at its most uncertain.

A further problem with AVHRR NDVI data is that of scale. A sensitivity analysis of the model to the changing scale of vegetation cover has shown that erosion can be reduced by orders of magnitude as the spatial scale of the vegetation cover estimate is reduced (Drake *et al.*, 1999). This reduction in erosion with progressively coarser scales is caused by a loss of variance. The negative exponential relationship between cover and erosion means that erosion is very high in bare areas but very low once cover exceeds around 40%. If we consider an image of vegetation patches (i.e. fields) with 100% cover, surrounded by bare fields, erosion is very high in bare areas and non-existent in the vegetated fields. When the spatial resolution of the image is reduced to a point when it exceeds the field size, predicted erosion is reduced because some of the vegetation cover of the vegetated field is assigned to the bare areas. To overcome this problem we have developed a method based on a polya function (Appendix 1), which provides more accurate results, but at the expense of reducing the spatial resolution of the image eightfold. It is not practical to apply the polya method to the 7.5 km ARTEMIS NDVI data as the resolution would be reduced to an unusable 60km. However, as the AVHRR LAC data is has a much better spatial resolution of 1 km, output from the LAC NDVI Polya function has a spatial resolution similar to that of the ARTEMIS data. Thus the polya function has only been applied during the real-time demonstrator section of the study, where 1km data was available.

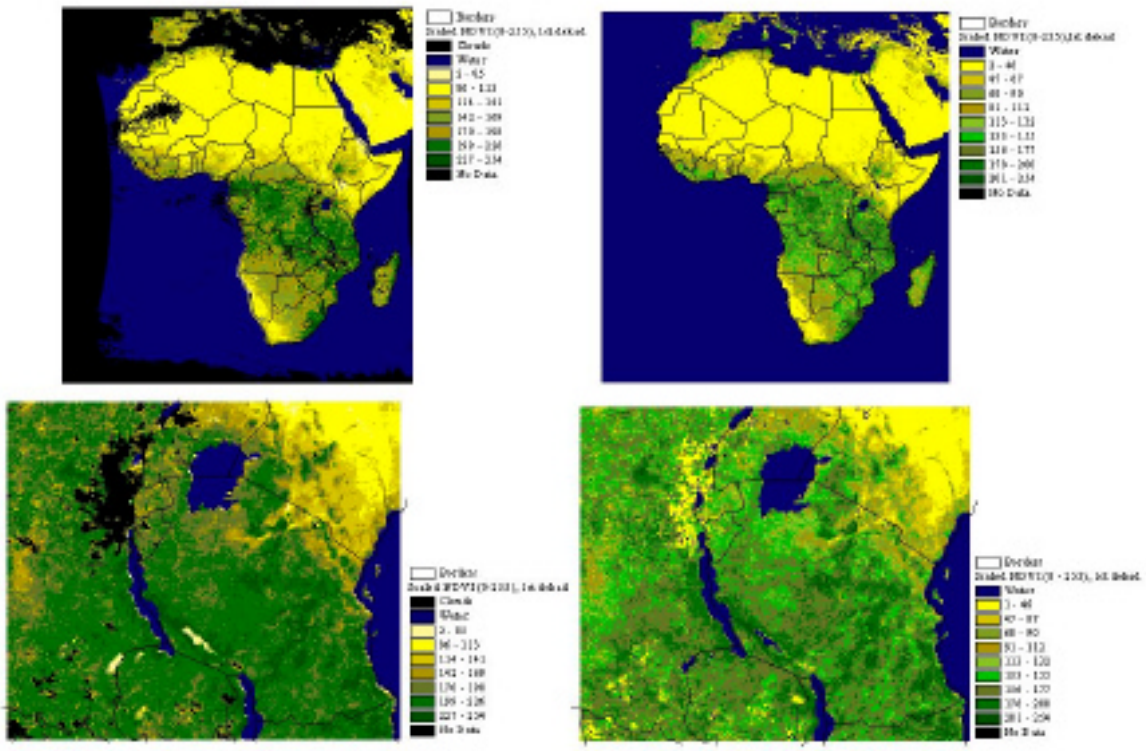

Figure 2. Example of the ARTEMIS decadal NDVI imagery. Each image contains gaps where there is cloud cover for the entire decad (black areas in the top left and bottom left images). These gaps are filled the with the average NDVI from the preceding and following decads (top right and bottom right images).

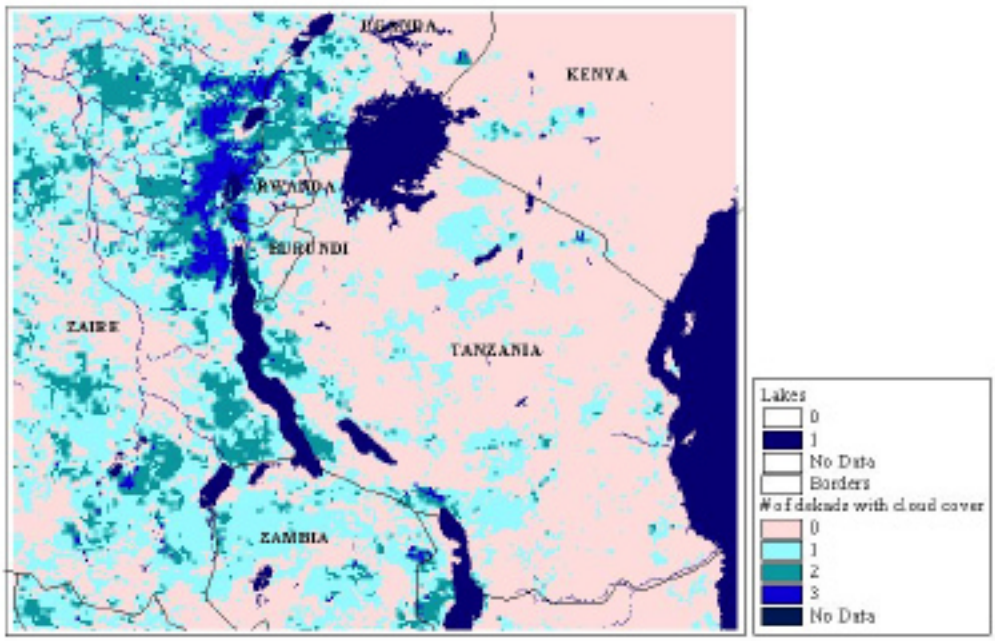

Figure 3. Decadal cloud cover. There are a few places in Zaire, Rwanda and Burundi where cloud cover exists for the entire month of March 1996.

3.1.2 Slope

Slope is estimated from the GTPO30 global 1km digital elevation model (DEM). The problem with calculating slope from Global DEMs is that it also suffers scaling problems being progressively underestimated at coarser scales. To overcome the problem a method has been developed for calculating slope as a function of scale using a fractal approach (Zhang *et al.*, 1999). Using the variogram technique to calculate the fractal dimension the difference in elevation between two points and the distance between them can be expressed by the following formula:

$$\left(Z_p - Z_q\right)^2 = \alpha\, d^{4-2D} \tag{3}$$

so that:

$$\frac{Z_p - Z_q}{d} = \alpha'\, d^{1-D} \tag{4}$$

where Z_p and Z_q are the elevations at points p and q, d is the distance between p and q, a and $\alpha' = \pm a^{0.5}$ are coefficients and D is the fractal dimension. Because the value $\frac{Z_p - Z_q}{d}$ is the surface slope it can be assumed that the percentage slope S is related to its corresponding scale (grid size) d by the equation:

$$S = \alpha'\, d^{1-D} \tag{5}$$

This result implies that if topography is fractal, then slope will be a function of the scale of measurement. Thus, the calculation of the local fractal properties permits the use of equation 4 to calculate slope at any specified scale d. The local fractal dimension describes the roughness of the topography while the local value of α is related to the concept of lacunarity which is a measure of the size of the gaps in a pattern. In terms of topography, the 'gaps' are the valleys and plains in the DEM.

To test this method we calculated the local (3X3 window) α and D from the 1 km DEM and then calculated slope for a d of 200 m and 30 m, compared them to two DEMs of this resolution and found RMS errors of 3.92% at 30m and 8.63% at 200m (Zhang *et al.*, 1999). The Fractal Topographic Slope map slope for the study area is shown in Figure 4. The map shows that there are a few problems with this DEM. In south-central Tanzania block shaped abrupt changes in slope suggest that the map sheets that make up the DEM do not fit together properly. We are, however, unable to make a correction for this at this time.

3.1.2 Soil Erodibility

Soil erodibility is estimated from texture and organic matter data contained within the 8 km resolution UNEP/GRID Digital FAO Soil Map of the World (Figure 5). We employed the table of Mitchel and Bubenzer (1980) (Table1) using Boolean Algebra to convert the soil map into spatially distributed K values. Because the soils are clay rich the map shows that soil erodibility within the catchment is generally quite low.

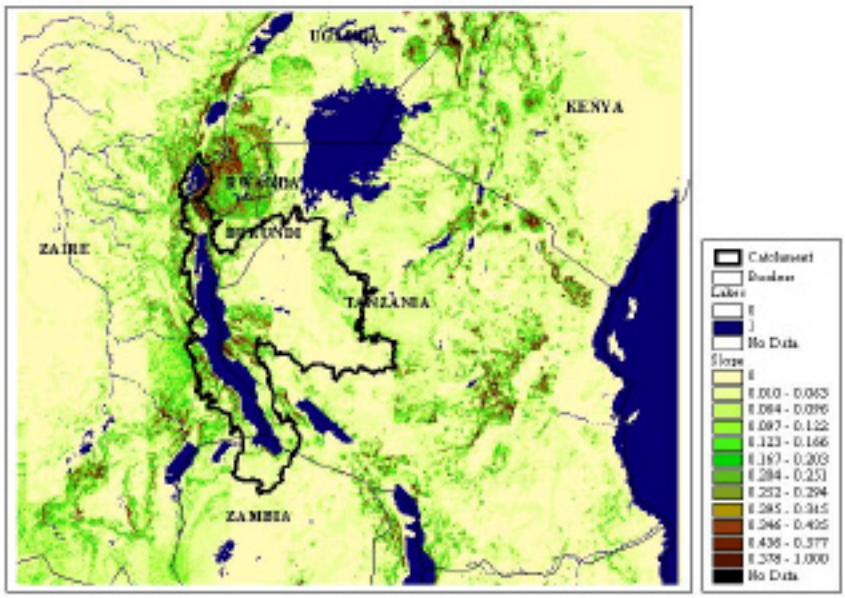

Figure 4. Fractal Topographic Slope map for the study area (degrees).

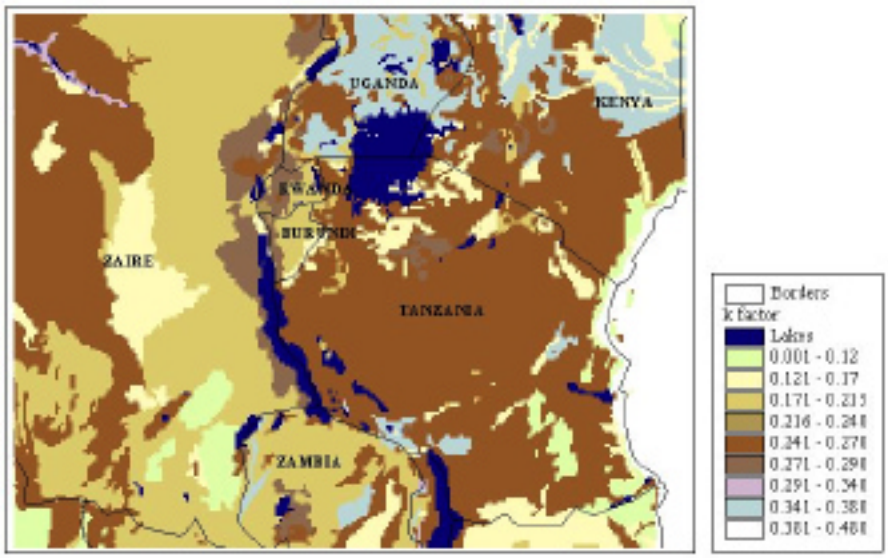

Figure 5. Soil erodibility estimated using the information provided in Table 1 from texture and organic matter data contained within the 8 km resolution UNEP/GRID Digital FAO Soil Map of the World.

TEX. CLASS	0.875 < %OM	0.875 <= OM < 1.625	1.625 <= OM < 2.5	2.5 <= OM < 3.5	OM >= 3.5
Sand	0.05	0.04	0.03	0.025	0.02
Loamy sand	0.12	0.11	0.1	0.09	0.08
Sandy loam	0.27	0.255	0.24	0.215	0.19
Loam	0.38	0.36	0.34	0.315	0.29
Silt loam	0.48	0.45	0.42	0.375	0.33
Silt	0.6	0.56	0.52	0.47	0.42
Sandy clay loam	0.27	0.26	0.25	0.23	0.21
Clay loam	0.28	0.265	0.25	0.23	0.21
Sandy clay	0.14	0.135	0.13	0.125	0.12
Silty clay	0.25	0.24	0.23	0.21	0.19
Clay	0.13	0.17	0.21	0.25	0.29

Table 1. The relationship between soil texture, organic matter and soil erodibility.

3.1.3 Overland Flow

The SCS model (Soil Conservation Service, 1972) has been used to estimate overland flow as the data to parameterise it are available for the study area, and it is both realistic and robust. The model was developed by studying overland flow in many small experimental watersheds. The basis of the model is that the ratio of overland flow (*OF*) to effective storm rainfall (Pe = P-Ia, where P is rainfall and Ia is initial abstraction) is equal to Fa/S where Fa is the water retained in the watershed and S the potential retention,

$$OFp = \frac{(r_i - Ia)^2}{(r_i + 0.8S)} \qquad (6)$$

where *OFp* is the overland flow in a rainfall event, r_i is rainfall, *Ia* = 0.2S, S is the potential retention $= \frac{25400}{CN} - 254$ (mm), and *CN* is the runoff curve number that can be estimated from published tables (e.g. Rawls *et al*., 1993). Estimation of curve numbers from these tables using GIS involves Boolean Algebra. Curve number estimation requires information on soil texture which is derived from the FAO Soil Map of the World (8km spatial resolution), landuse which is derived from the IGBP Global 1 km Landuse Map (Figure 6a) and was reclassified so that it corresponded with the SCS landuse categories (Figure 6b), and vegetation cover derived from NDVI imagery (ARTEMIS 7.5km, Figure 2). The curve number describes the ability of the pixel to produce runoff, with high curve numbers providing ideal conditions for runoff generation. These curve number maps are dynamic on a dekadal basis since they change according to variations in vegetation cover.

3.1.3.1 Parameterisation of Rainfall in the SCS Model

The contract proposed parameterisation of the overland flow model with two types of rainfall data in order to determine which is most appropriate for continued operational monitoring. Firstly, interpolated World Meteorological Organisation (WMO) Global Telecommunications System (GTS) raingauge station measurements, which consist of daily records from 760 raingauges throughout Africa (Figure 7a); and secondly 10-day satellite-derived precipitation estimates produced by the US Aid Famine Early Warning System (FEWS). In addition to this

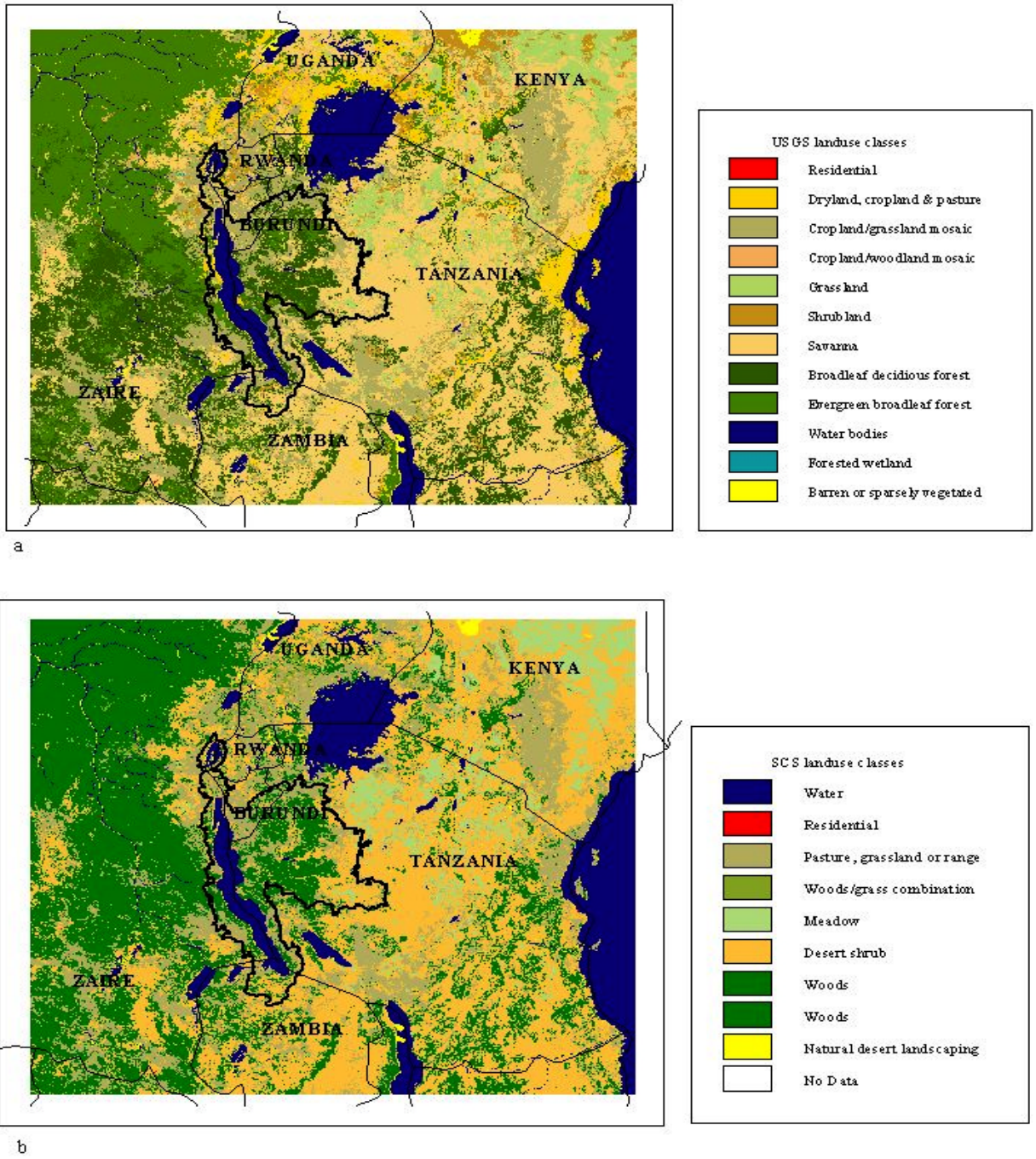

Figure 6. Landuse and SCS class maps for the study area. A) USGS/IGBP Global 1 km Landuse Map. B) Reclassification of IGBP to SCS classes.

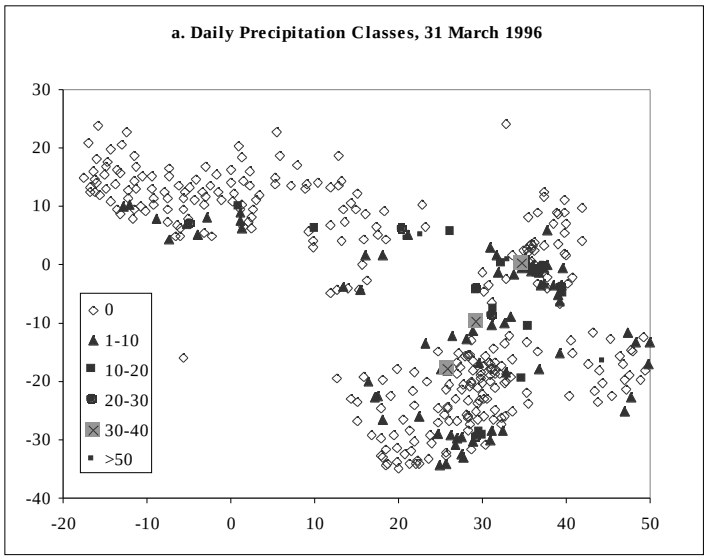

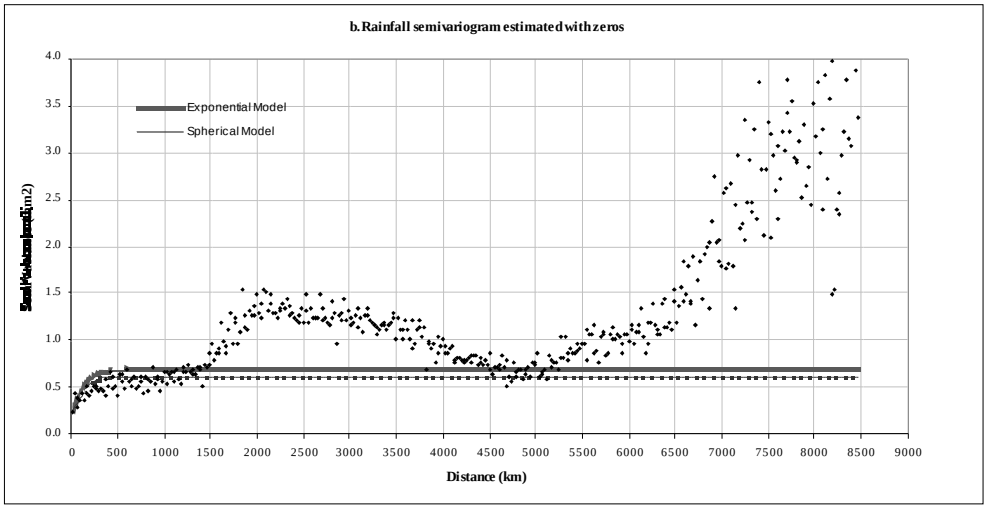

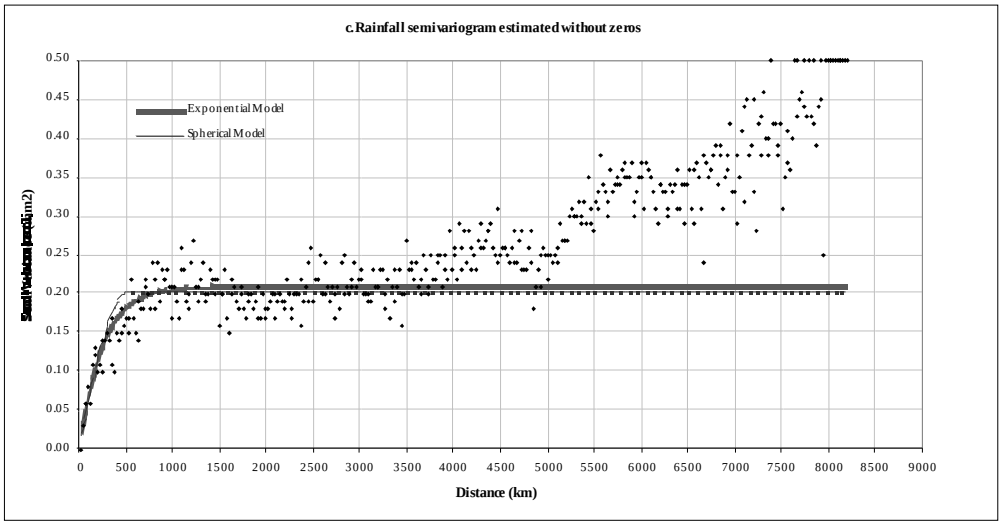

Figure 7. A) Distribution of daily rainfall over sub-Saharan Africa for 31st March 1996. B) Sample semi-variogram estimated with zero values; and C) without the zero values.

we have also evaluated the utility of incorporating additional raingauge data, purchased from the national meteorological offices of Burundi, Kenya, Tanzania, and Zambia (from now on referred to as BKTZ) along with that obtained via the GTS.

These two data sources have advantages and limitations in terms of both spatial detail and temporal resolution. GTS data are worse than FEWS spatially since the raingauge network is relatively sparse in many areas and many stations do not get posted on the GTS. Furthermore, there are many gaps in the individual GTS station records, which do not occur in the FEWS data. However, in terms of temporal frequency GTS data is acquired on a daily basis whereas the FEWS data is dekadal. Because the SCS model is event based it is directly applicable to daily data and cannot be applied to dekadal data without additional development (See Section 3.1.2.4).

The accuracy of the GTS data, GTS+BKTZ data, and the FEWS data was assessed for March 1996 using 1942 independent stations from South Africa. In addition, the 56 BKTZ stations were also used to evaluate the accuracy of the GTS and FEWS data for east Africa.

3.1.3.2 Interpolation Using Kriging

After much experimentation we found that the most accurate method for implementing kriging was by using a combination of ordinary and indicator kriging. Although kriging has been shown to provide better results than the classical methods (e.g. Thiessen polygons, polynomial or spline fitting, etc.), questions arise concerning the statistical assumptions made: kriging provides the best possible estimate when the set of variables is multigaussian, but when intermittency of rainfall prevails the frequency distributions exhibit a jump at 0. This is clearly shown with the semi-variogram, which is a statistical way of quantifying the spatial variation of the data. The semi-variance is estimated by the sample semi-variogram, the value of which for a station separation-distance of h, is the average squared difference in the amount of rainfall between pairs of stations separated by h. The sample semi-variogram was calculated from the data with Equation 1:

$$\gamma(h) = 1/(2n) \sum \{ Z(x_i) - Z(x_i + h)\}^2 \qquad (5)$$

where *n* is the number of pairs of stations separated by distance *h*.

Figures 7b and 7c show variograms for the GTS gauge data set for the 31st March 1996 - one derived considering all values (Figure 7b), the other derived from the non-zero rainfall values only (Figure 7c). The difference between the two clearly shows how the semi-variogram is swamped by the variability associated with the zero values in two ways:
1. close to the origin, i.e. for distances up to about 1000km, it decreases the semi-variance (for the same distance) since zero-value pairs contribute zero semivariance, and;
2. at medium distances (1500-4000km), it causes a pronounced increase in the semivariance. This occurs because on average these distances correspond to stations pairs which are too far apart to belong to a continuous dry or continuous wet area (Figure 7a). Therefore, "the departure from normality results from the intermittentcy, and practically vanishes when zero and non-zero rainfall values are processed separately" (Barancourt and Creutin, 1992).

To overcome this problem the zero events were excluded and semi-variograms were estimated using a lag distance *h* of 100km. The semi-variograms were then modelled by fitting two different theoretical functions to them by maximum likelihood: a spherical and an exponential (Equations 6 and 7):

$$\gamma(h) = \sigma^2 (3h/2r - h^3/2r^3) \text{ for } h \le r$$
$$\gamma(h) = \sigma^2 \text{ otherwise} \quad (6)$$

$$\gamma(h) = \sigma^2 (1 - e^{-3h/r}) \quad (7)$$

where r is the range and σ^2 is the sill (Baily and Gatrell, 1995). The model with the lowest likelihood was selected. Ordinary kriging was then applied to produce an areal rainfall map which inevitably has non-zero values over the dry areas. Indicator kriging was then applied to the entire set of values (i.e. including the zeros). The result of this, is a field valued between 0 and 1, which can be seen as the probability of an x,y location being wet. By defining a probability level of 50% this field was transformed to a binary one, with ones where rain occurred and zeros where it did not. The multiplicative combination of these two results provided the desired estimator of mean areal rainfall. This method has been shown to be more accurate than using ordinary kriging alone (Baily and Gatrell, 1995).

3.1.3.3 The Satellite Precipitation Estimates

The 10-day FEWS satellite precipitation estimates are developed as follows: a preliminary estimate of accumulated precipitation is made based using the GOES Precipitation Index (GPI), an algorithm developed for the USA by Arkin and Meisner (1987), with Meteosat imagery collected over the African Continent. The GPI uses the duration of cold cloud tops over a region for the determination of accumulated rainfall (3mm of precipitation for each hour that cloud top temperatures are measured to be less than 235^oK). The GPI estimate is corrected using a bias field that is calculated by incorporating the GTS observational data and fitting the biases to a grid using optimal interpolation producing an estimate of convective rainfall. Over regions in which precipitation is due to orographic lifting and the clouds are relatively warm, an additional procedure is used which incorporates the local terrain features with numerical model analyses of meteorological parameters. This process for warm cloud precipitation estimation takes into account surface wind direction, relative humidity and terrain. The combined technique incorporates rainfall from both the convective and stratiform cloud types, producing a final estimate of total accumulated precipitation.

3.1.3.4 Development of the SCS Model for FEWS data

The main problem of implimenting the SCS model with the FEWS rainfall estimates is that the model is only applicable for rainfall events. To overcome this the model was adjusted to run on a dekadal basis (Zhang *et al.,* 1999) where *OF(i)* is calculated in the following manner:

$$OF(i) = \sum_{i=1}^{n} \Delta r OFpJ \quad (8)$$

OFp is overland flow per n where there are *n* different classes of rainfall intensity, *i*=1...n,

$$\Delta r = \frac{(r_{max} - Ia)}{n} \quad (9)$$

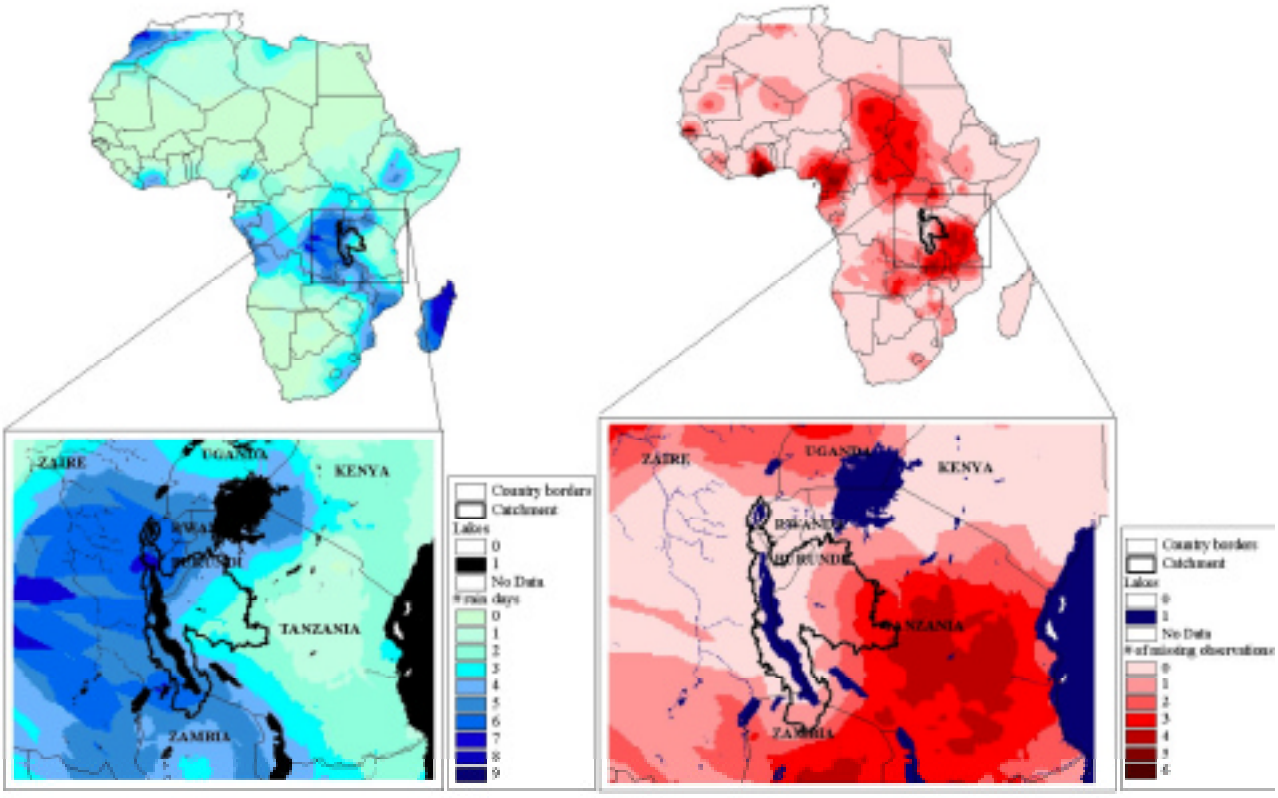

Figure 8. The number of rain days per decad calculated from the GTS station data. Left) Interpolation of rain days using kriging. Right) Interpolation of the missing data in each decad using kriging.

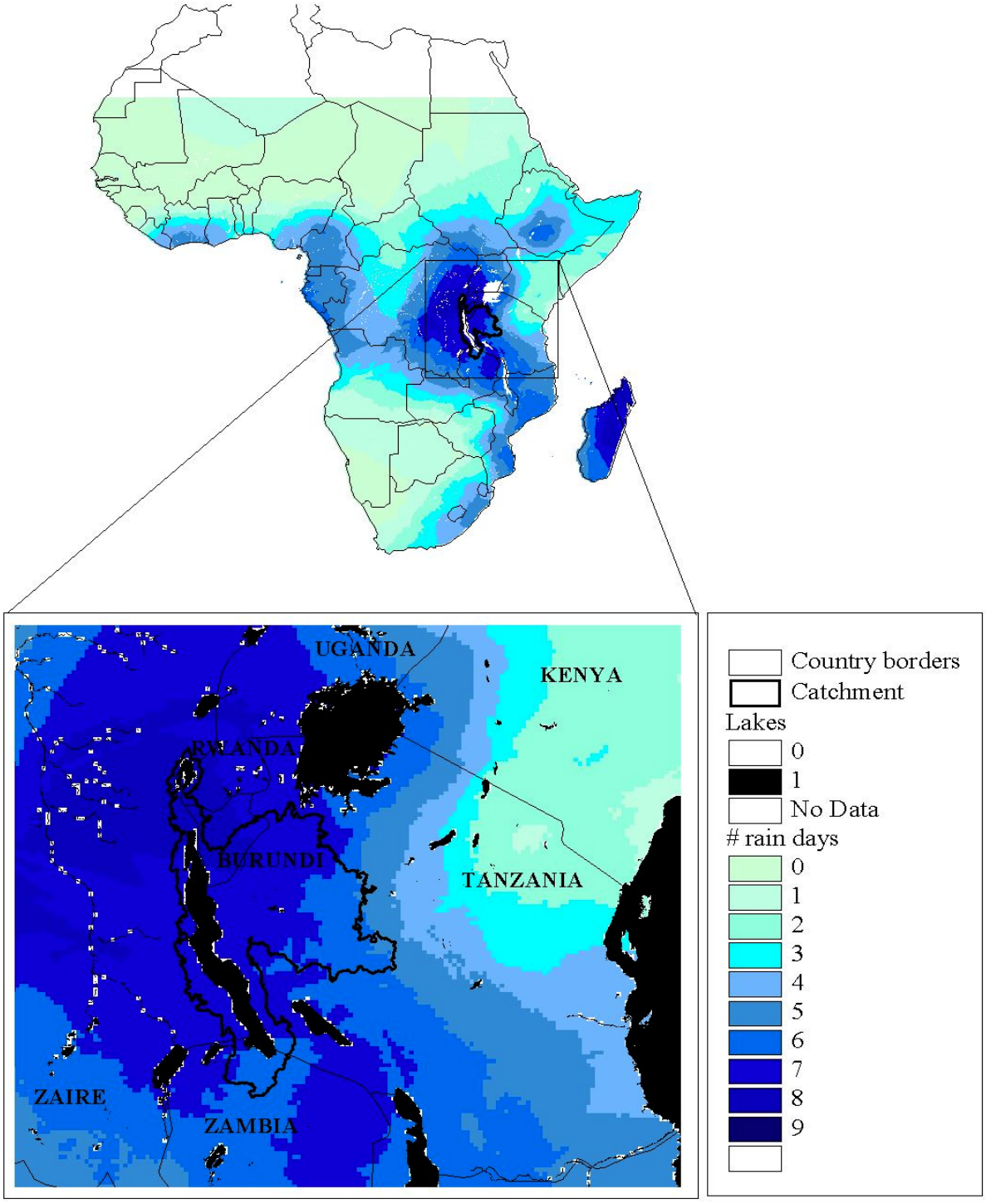

Figure 9. The number of rain days per decad calculated using indicator kriging of daily GTS data.

r_{max} is the maximum rainfall per rain day which is assumed to be 500 mm, and *J* is the rain day frequency density function which is assumed to be:

$$J = \frac{Jo}{ro} e^{-\frac{r_i}{ro}} \quad (10)$$

where *Jo* is the total number of rain days per month, r_i is the rainfall per rain day and *ro* is the mean rainfall per rain day (mm).

Though this methodology allows the use of FEWS data in the overland flow model, GTS data are still needed since a map of the number of rain days per dekad is required. We have produced this by interpolating the GTS data.

3.1.3.5 Estimation of Rain Days

The number of rain days per dekad can be calculated from the GTS station data by simply summing the number of days that rain occurs during a particular dekad and interpolating this data using Kriging (Figure 8). However, the GTS data contains much missing data in each dekad (Figure 8), and thus for many days in each dekad we do not know if it actually rained or not. This problem is particularly acute in Tanzania where there is a large amount of missing GTS data, but the map needs to be interpreted with caution since the Democratic Republic of Congo reports no rainfall stations to the GTS network and so records no missing data. The problem of missing data is reduced if we apply indicator kriging to the GTS data in order to produce a map of where it rained on each day and then sum these maps to dekads. This is a better methodology because we can interpolate into areas where data is missing. This methodology produces more raindays in the lake catchment than the previous method (Figure 9).

4. Results

4.1 Comparison of FEWS and Interpolated GTS and BKTZ Data

We have evaluated the accuracy of dekadal rainfall for the kriging interpolations using GTS data, GTS plus the additional rainfall station data (5 from Zambia, 21 from Kenya, 5 from Tanzania and 24 from Burundi: BKTZ) and the FEWS data. To compare the FEWS and interpolated data, the daily data is summed to dekads. Figure 10 shows the dekadal FEWS data, the interpolated GTS data, and the GTS plus the BKTZ stations for the second dekad of March 1996 for the whole of Sub-Saharan Africa. Figure 11 shows the predicted rainfall within the catchment in more detail. We have presented data for the whole of Sub-Saharan Africa for two reasons. Firstly, part of our validation uses data from South Africa. Secondly, for the rainfall interpolations stations outside the Lake Tanganyika catchment affect the predicted rainfall within it.

There are notable differences between the three rainfall estimates with the kriging data containing much less spatial detail than the FEWS data. In the FEWS image large storm cloud structures are visible and higher rainfall is predicted in many areas, particularly over Democratic Republic of Congo. The GTS plus BKTZ data seems to provide a considerable

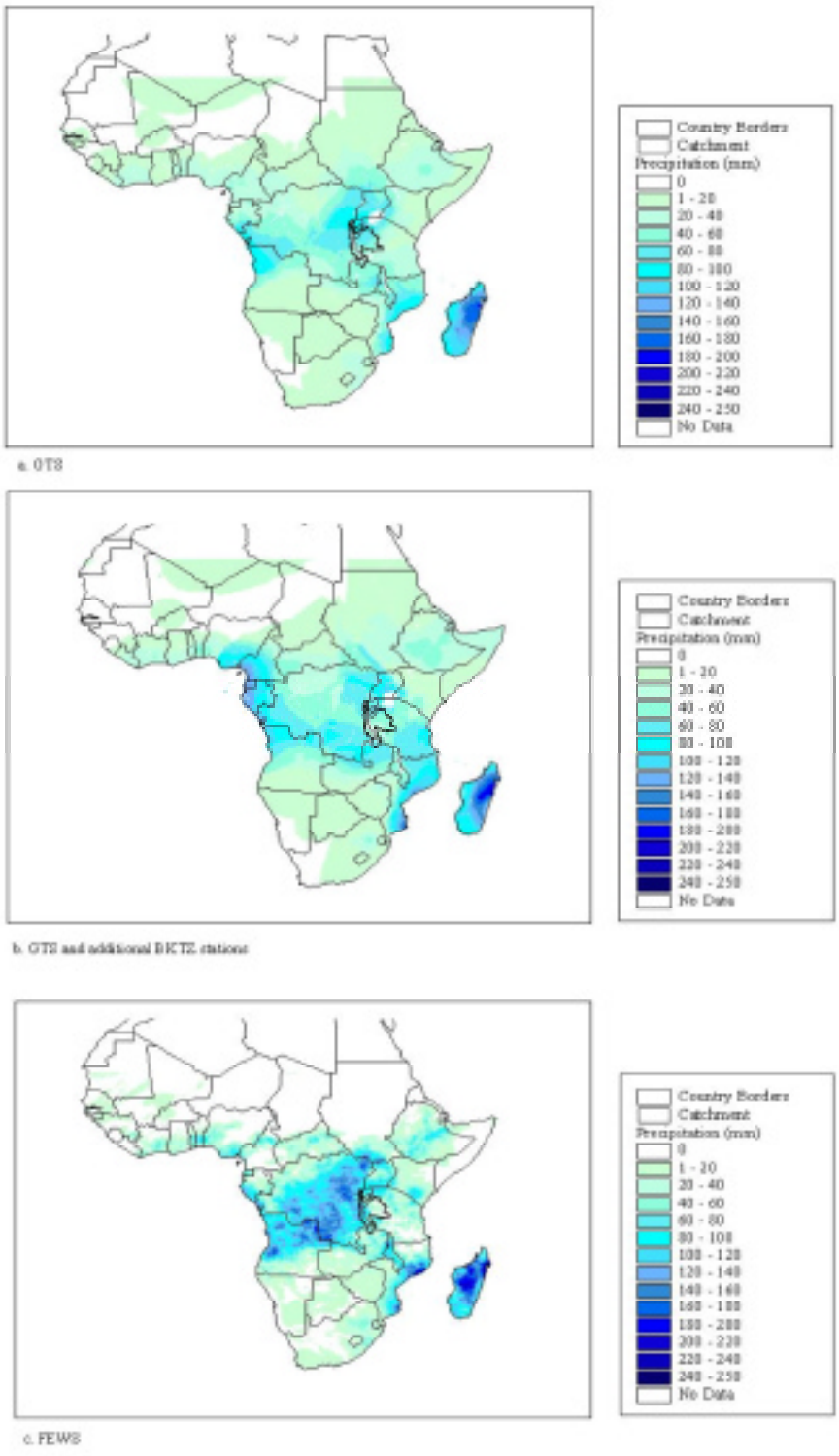

Figure 10. FEWS and interpolated GTS data for the second decad of March 1996 for the whole of Sub-Saharan Africa.

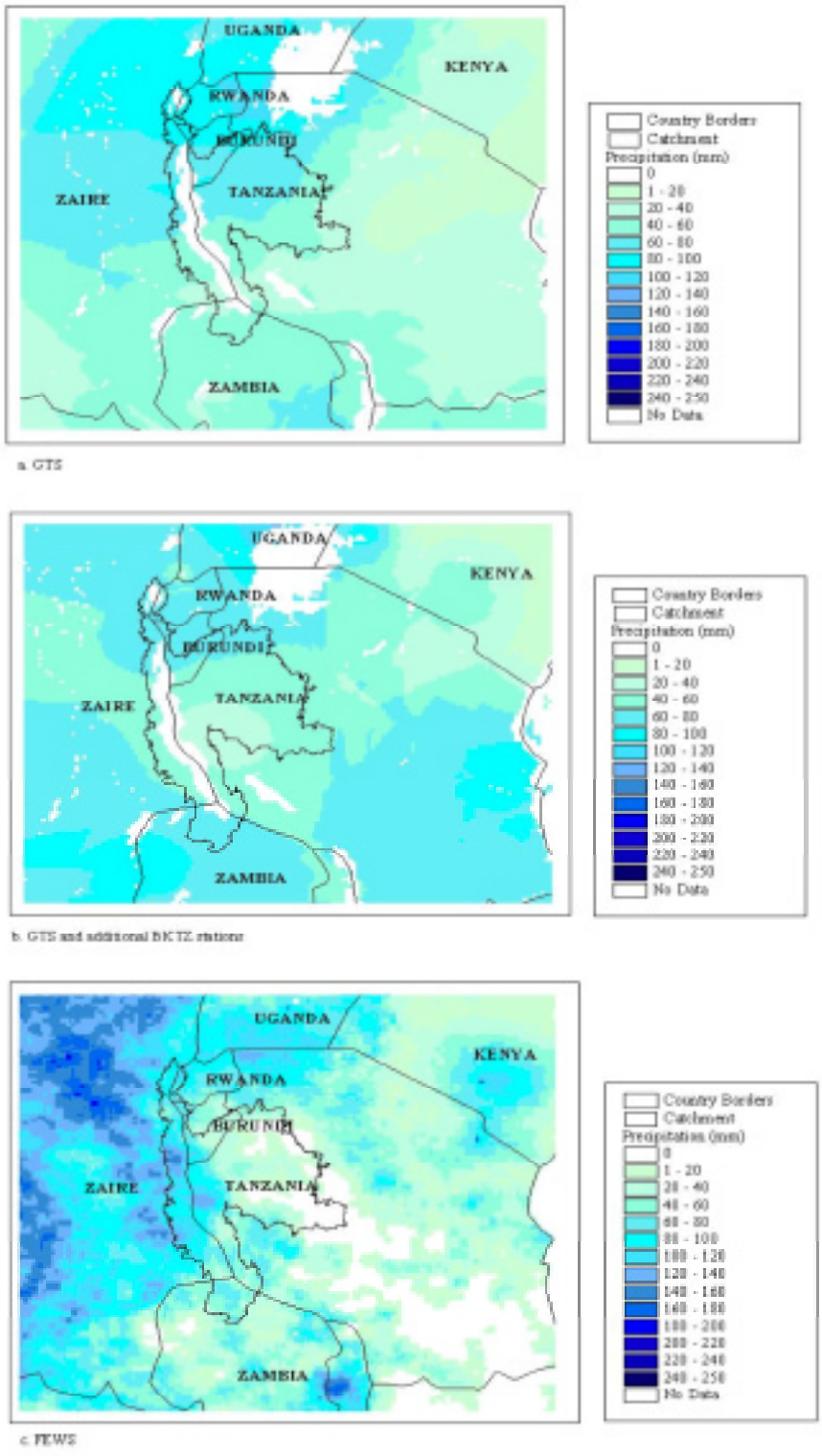

Figure 11. The Lake Tanganyika catchment shown in more detail. FEWS and interpolated GTS data for the second decad of March 1996.

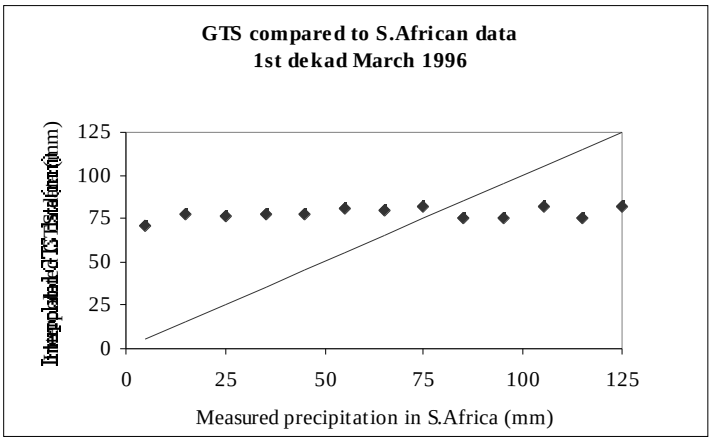

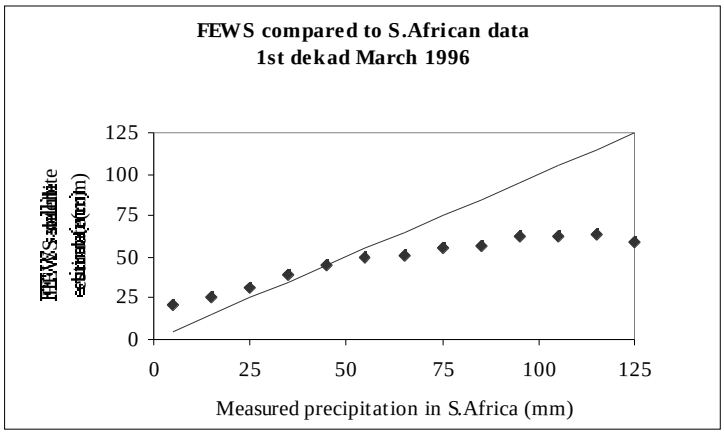

Figure 12. Measured South African precipitation against interpolated GTS and FEWS. The diagonal line is the 1:1 line.

	1st Dekad	2nd Dekad	3rd Dekad
RMS_{GTS}(mm)	57.1	17.0	11.3
RMS_{BKTZ} (mm)	47.5	18.5	11.4
RMS_{FEWS} (mm)	24.4	17.5	11.2

Table 2. RMS errors for the interpolated GTS data, the interpolated GTS plus BKTZ stations and the FEWS satellite estimates for South Africa during March 1996.

improvement on the interpolated GTS rainfall data alone and, for the date shown, predicted rainfall within the lake catchment is quite significantly altered.

Two points need to be considered in order to assess the accuracy of the three datasets, (i) spatial detail, and (ii) the accuracy of the rainfall totals. In spatial terms the FEWS rainfall estimates appear better. In areas where the GTS network is relatively dense and rainfall is occurring the interpolated data often overestimates areas experiencing low amounts of rainfall due to the smoothing associated with interpolation. Furthermore, large differences occur where the network is sparse (i.e. northern Democratic Republic of Congo) because storms are unrecorded, and again in these regions FEWS data is probably more reliable. The most significant difference between these data occurs in Democratic Republic of Congo

where there are few rainfall stations but considerable rain is mapped by the FEWS Meteosat based method.

In order to quantitatively investigate the accuracy of these different rainfall datasets RMS errors were estimated for the independent South African stations and the BKTZ stations (Tables 2 and 3). Furthermore, predicted values were graphically compared to the independent raingague data (Figure 12).

	1st Dekad	2nd Dekad	3rd Dekad
RMS_{GTS} (mm)	36.17	37.07	34.42
RMS_{FEWS} (mm)	30.16	35.23	39.60

Table 3. RMS errors for the interpolated GTS data and the FEWS satellite estimates at the additional BKTZ stations during March 1996.

PRECIP.CLASS	Average measured South African	Average estimate of FEWS for South African	RMS of FEWS for South African	RMS Herman et al 1997 for the Sahel
15	14.17	25.02	17.76	5
25	24.30	30.82	16.88	10
35	34.69	38.93	16.66	15
45	43.87	45.59	17.94	17
55	53.89	49.22	16.12	20
65	63.93	51.39	21.70	21
75	74.04	56.02	25.08	22
85	83.92	56.63	32.35	23
95	93.74	63.03	32.97	25
105	103.50	62.69	44.65	27
115	115.00	63.24	53.21	30
125	124.57	59.07	66.13	30
			average: 30.12	20.42

Table 4. Comparison of errors associated with FEWS rainfall for South Africa and the Sahel.

The results show that higher rainfall rates produce larger RMS errors and bigger differences in estimated rainfall between the different techniques, which is a potentially important observation. In South Africa (Table 2 and Figure 12) there is little difference between the techniques when rainfall is low (i.e. dekad 2 and 3), but at times of high rainfall (i.e. dekad 1) kriging is insensitive to any actual spatial rainfall variations. This could be explained by high spatial variability in the actual rainfall that is not represented in the semi-variance of the relatively sparse GTS raingauge network. In general the FEWS images are more accurate than kriging (in terms of RMS error), especially for precipitation values up to 60mm. Though from 60mm upwards FEWS also seems to be underestimating rainfall in South Africa (Figure 12).

The results from the comparison with the data from Burundi, Kenya, Tanzania and Zambia (BKTZ, Table 3) show that FEWS is marginally better in the first two dekads but, also

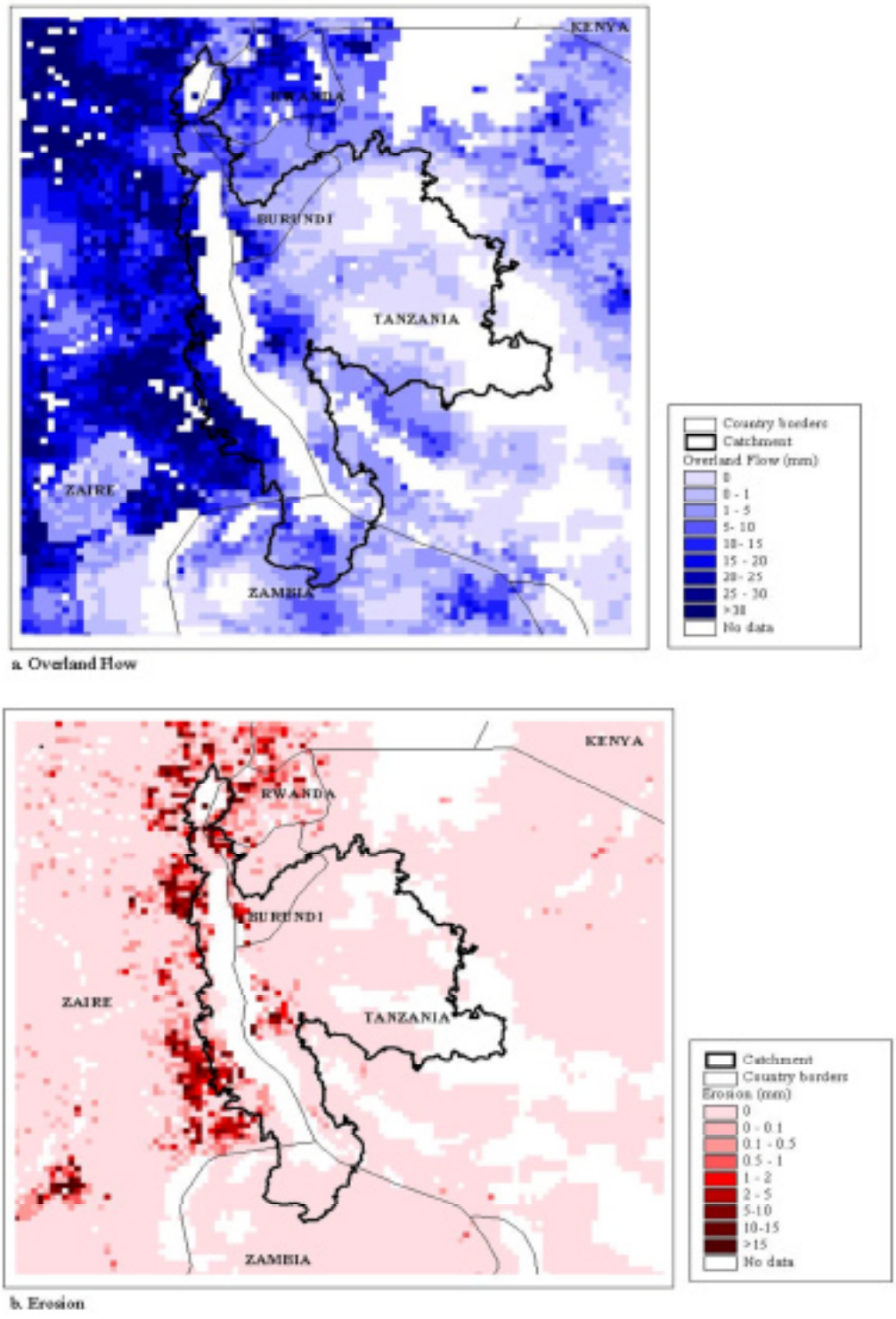

Figure 13. Overland flow and erosion estimated with FEWS rainfall inputs for the second dekad of March 1996.

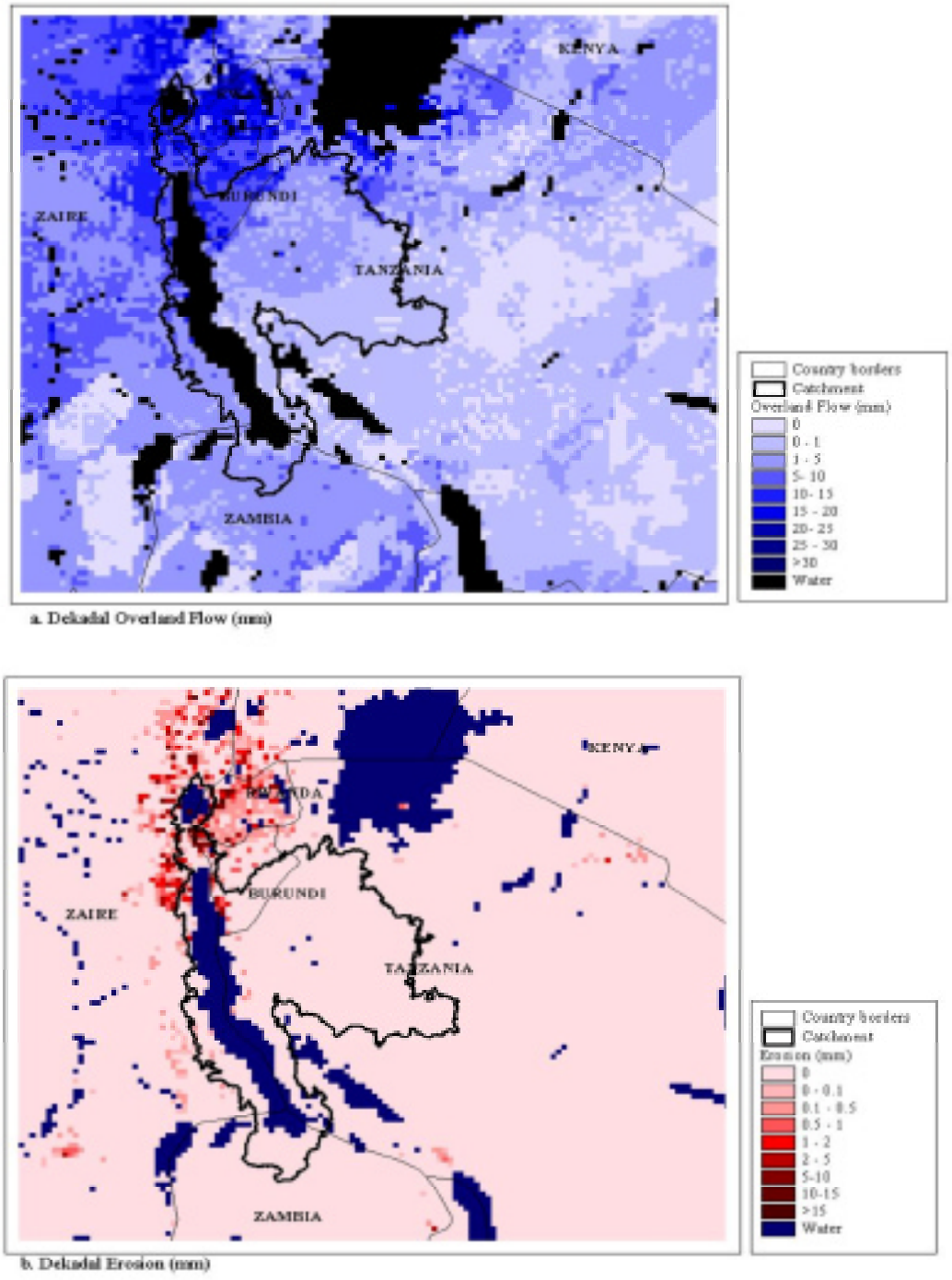

Figure 14. Overland flow and erosion estimated using the interpolated GTS data for the second dekad of March 1996.

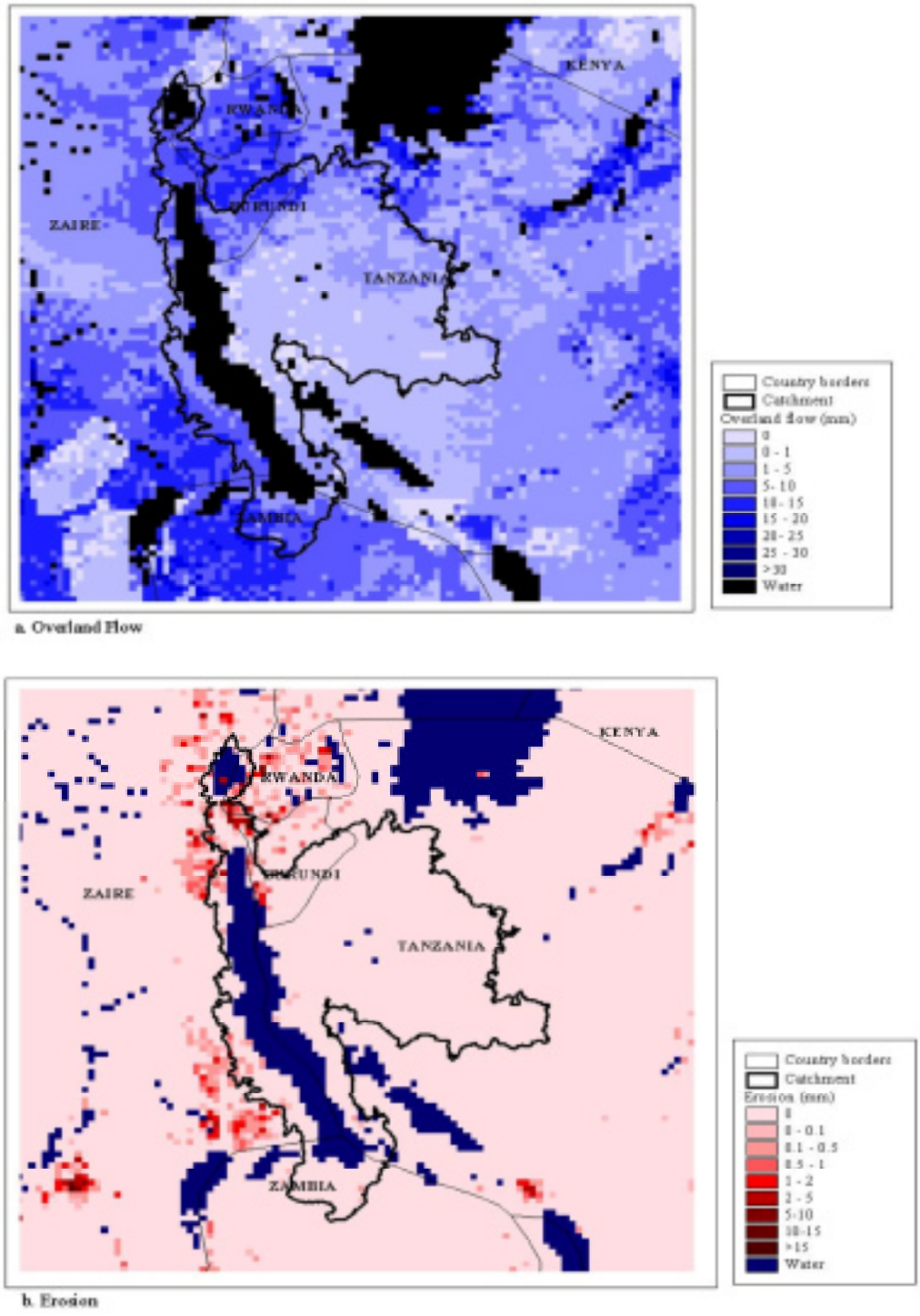

Figure 15. Overland flow and erosion estimated using the interpolated GTS plus BKTZ data for the second dekad of March 1996.

marginally, worse in the third. Thus there seems to be little difference in the accuracy of the techniques in this region even though FEWS data shows considerably more spatial detail. Herman *et al.,* (1997) conducted an evaluation of the FEWS algorithm for June to September 1995 for Mali, Niger and Chad. They found an average RMS error of about 22mm which is similar to many of our findings. However, a comparison of our South African validation to theirs for the Sahel for different intensities of rainfall shows that the errors associated with the South African data are always larger (Table 4).

In conclusion, though in East Africa area there is little difference between interpolated GTS and FEWS data, in South Africa FEWS appears to be superior but the errors we found are slightly higher than those of Herman *et al.,* (1997). The use of additional raingauges improves the results of the interpolation but the RMS errors are still higher than that of the FEWS data. Furthermore, we have only validated the rainfall estimates in areas with a relatively high raingague density. In regions where the network is sparse (e.g. Democratic Republic of Congo and Angola) the difference between FEWS and the interpolated data is large and FEWS is likley to be much more accurate in these regions where there are few raingauges to use for interpolation. Because an important part of the Lake Tanganyika catchment is located in Democratic Republic of Congo FEWS is almost certainly the most accurate data source.

4.2 Effect of Different Rainfall Estimates on Overland Flow and Erosion

Figure 13 shows overland flow and erosion estimated with FEWS for the second dekad of March 1996, Figure 14 shows overland flow and erosion estimated using the interpolated GTS data, and Figure 15 shows overland flow and erosion estimated using the interpolated GTS plus BKTZ data. This is the dekad when the highest rainfall, overland flow and erosion occurs in March 1996.

Both the magnitude and the spatial patterns of overland flow and erosion differ between these three model parameterisations. Overland flow and erosion estimated with the use of the FEWS data (Figure 13) is spatially more extensive than that estimated with the GTS data (Figures 14 and 15), however, there are also significant differences between the GTS and GTS plus BKTZ overland flow and erosion estimates. Big differences are found in south-east Democratic Republic of Congo where the GTS data predicts little overland flow and erosion, the GTS plus BKTZ predicts a little more and the FEWS data predicts a considerable amount. These differences can be explained by two factors. Firstly, increased overland flow and erosion is caused by the fact that FEWS precipitation estimates are higher. Secondly, the vast majority of the areas where FEWS data predicts overland flow and erosion but kriging does not are located in Democratic Republic of Congo where the GTS network is very sparse and rainfall is underestimated by the kriging.

	Mean Rainfall (mm/dekad)	Mean Overland Flow (mm/dekad)	Mean Erosion (mm/dekad)
GTS	21.8	1.4	0.010
GTS+BKTZ	23.3	3.0	0.019
FEWS	31.5	6.2	0.086

Table 5. Mean rainfall, overland flow and erosion for Sub-Saharan Africa using the different rainfall estimates.

Table 5 sumarises the effect of the different rainfall parameterisations on average overland flow and erosion in Sub-Saharan Africa. FEWS rainfall estimates are higher than kriging using GTS and GTS plus BKTZ, though GTS plus BKTS is higher than GTS alone because there are less zero values. The different rainfall parameterisations have significant effects on predicted overland flow and erosion with the FEWS overland flow estimates being about 4 times higher than GTS and erosion estimates are 8 times higher. These large differences occur because rainfall is squared in the overland flow model and overland flow is also squared in the erosion model.

In terms of the spatial pattern of erosion, it is located in areas of low vegetation cover, high rainfall, overland flow, and slope; the classic situations that lead to high erosion rates. Erosion seems to be largely restricted to Rwanda, Burundi and Democratic Republic of Congo and one small part of Tanzania (Figure 13). Both Democratic Republic of Congo and Zambia suffer high rainfall and overland flow in both mountainous and lowland regions, however, within Rwanda, Burundi and Tanzania rainfall and overland flow are generally concentrated only in mountainous areas, as these are the only regions that generate significant rainfall. When it is considered that slopes are also high in these regions, that they tend to be densely populated, and thus vegetation cover is being reduced by human interference, it goes a long way to explaining the high erosion predicted in these regions.

In summary, the model appears to be very sensitive to the different spatial rainfall inputs and those obtained from FEWS appear to be the best for our purpose.

4.3 Evaluation of Model for Long Term Monitoring

The evaluation of the best method for spatial parameterisation of rainfall took much longer than anticipated, partly because we acquired more rainfall station data than we initially planned, and partly because a considerable amount of time was spent on determining the optimal method for kriging rainfall and rain days. Unfortunately the best way to estimate rain days involves indicator kriging of daily GTS data. Therefore we have to apply this methodology to 182 days of data and this is proving time consuming simply in terms of computing. Thus we have not yet completed the application of the soil erosion model for the entire wet season. This is currently being accomplished.

4.4 Catchment Sensitivity to Erosion and Scenarios of Landuse Change and Land Degradation

4.4.1 Sensitivity to Erosion

Defining areas within the catchment that are most sensitive to erosion has been accomplished by subjecting the catchment to an intense rainfall event and calculating the resultant erosion. Rather than arbitrarily determining a rainfall intensity it has been defined by calculating a rainfall return period. Rainfall return periods are notoriously susceptible to missing data. Thus we decided to select a rainfall station in (or near) the study area that had the best record (i.e. a long term record with small amounts of missing data). The station that satisfied these criteria best was Dar es Salaam airport. We used a five year record of daily data (1994-1998, 1825 records, 221 missing days) to estimate a two year rainfall return period of 160mm.

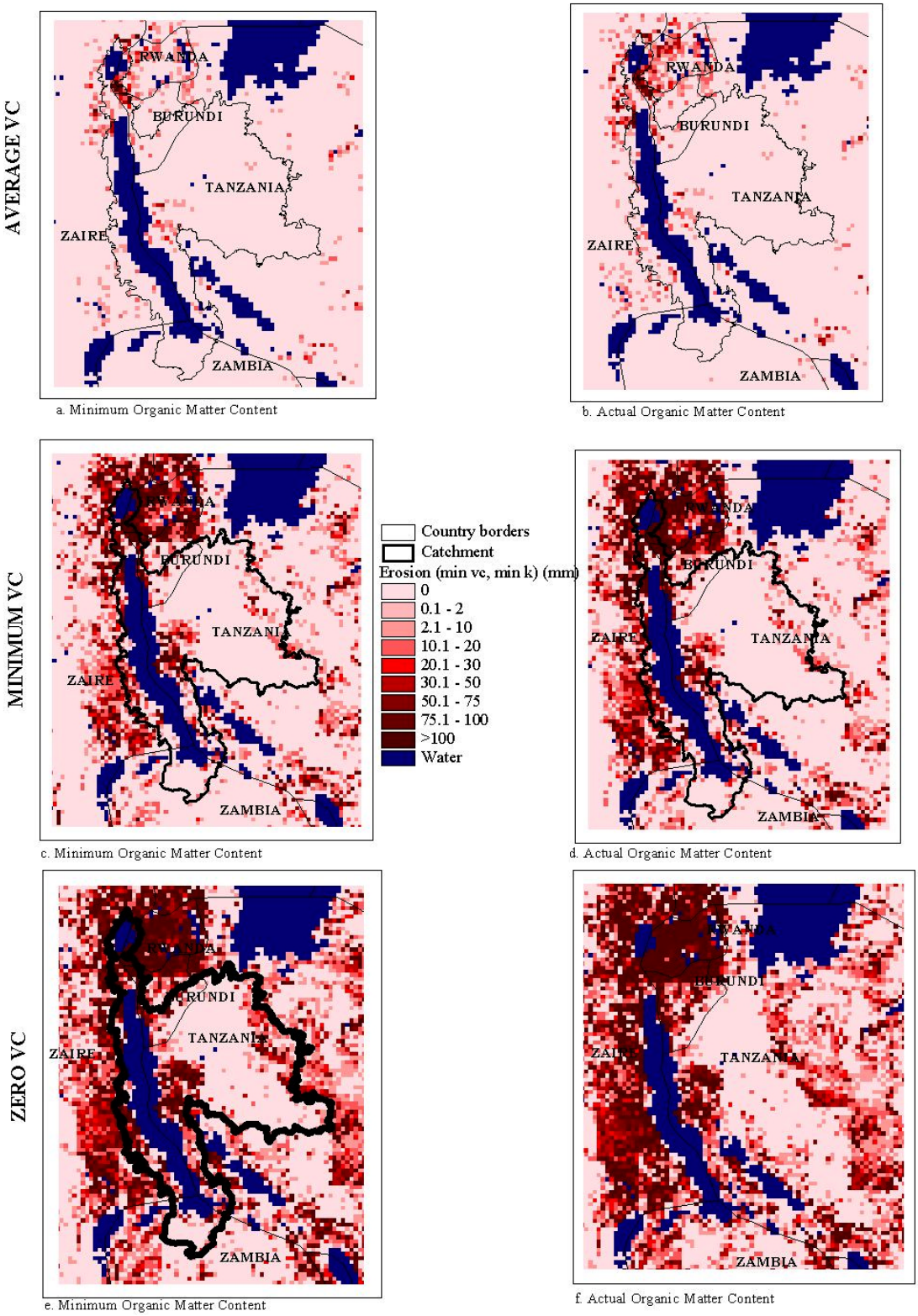

Figure 16. Catchment sensitivity to erosion, scenarios of deforestation and land degradation. See text for details.

The model was then run with this rainfall intensity in order to determine which areas suffer most strongly from erosion caused by extreme rainfall events. We calculated average vegetation cover from the ARTEMIS NDVI archive for 1996 in order to assess erosion sensitivities in this 'average' situation (Figure 16b). The reader should note that the magnitude of predicted erosion under these modelled 'very high rainfall' conditions is impossibly high. It appears that under extreme conditions such as these the model over predicts erosion due to the empirical relationships described by the model breaking down under these extreme conditions. Thus the results should be interpreted as simply indicating those areas that are more or less susceptible to erosion.

There are numerous small areas that are sensitive in this average cover situation. However, within the Lake Tanganyika catchment there is only one large area in western Burundi appears to be very highly susceptible to erosion. This is because it always appears to experience low vegetation cover. This region also suffered high erosion in March 1996 (Figure 13).

In summary, under average vegetation conditions few parts of the catchment are highly sensitive to erosion. However, drought, land degradation and inappropriate farming practices can cause a reduction in vegetation cover that may make parts or all of the catchment more susceptible to erosion in the future.

4.4.2 Land Degradation

Land degradation modelling allows identification of areas within the catchment that are most sensitive to degradation. We have implemented scenarios that consider the resilience of the soil and vegetation cover.

1) Vegetation Cover Degradation Due to Drought or Clearance.

A situation that causes increased soil erosion is when heavy rainfall occurs when vegetation cover is low. Low cover may be caused by extended drought, fire, clearance, or poor agricultural practices. This situation has been modelled by going through the ARTEMIS NDVI data archive and for each month of the 1996 and calculating the minimum NDVI for each pixel. We then subject this minimum vegetation cover to the two year return period rainfall event and model the resultant erosion.

Figure 16d shows the results of the scenario. It is clear that many areas of the catchment are susceptible to vegetation degradation in 1996, with localised hot spots in Burundi, Rwanda, Tanzania and Democratic Republic of Congo. These hot spots are similar in location to those that were found to be eroding in March 1996 (Figure 13).

2) Changing Soil Erodibility Caused by Reduced Organic Matter

Dejene *et al.*, (1997) show that in Tanzania soil organic matter can be exhausted within 10 years in areas that experience poor agricultural practices or high fire intensity and/or frequency. A reduction in soil organic matter generally increases soil erodibility for sandy soils, but can decrease it for clay rich soils. To model this soil degradation process we used the information in Table 1 to reduce the soil organic matter to less than 1 %, in order to simulate the soil degradation that would occur if poor practices were used. We then recalculated soil erodibility. The model was then implemented with the minimum vegetation cover and a two year rainfall return period outlined above.

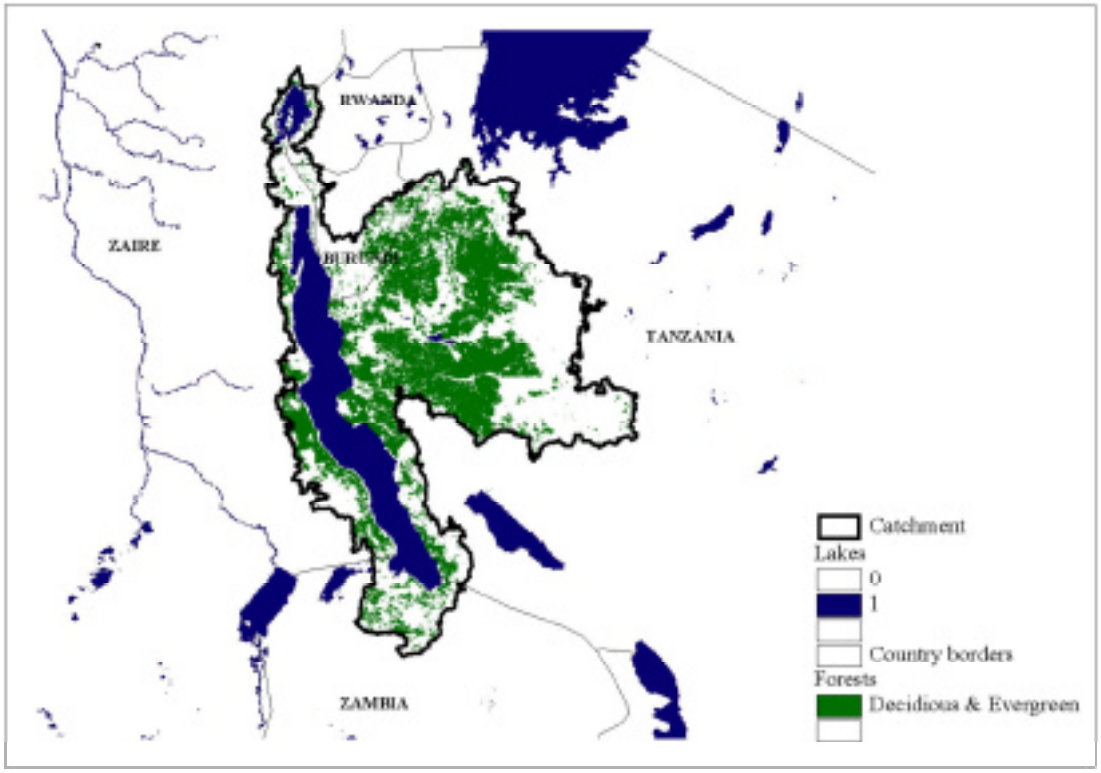

Figure 17. Forest cover map for the Lake Tanganyika Catchment derived from the IGBP landcover map.

The results are shown in Figure 16c. We find that reducing organic matter provides less erosion because the soils of the lake catchment are generally clay rich and their erodibility decreases when organic matter is reduced. Thus soil degradation seems to reduce erosion in the region. This suggests that the erosion provides potentially the greatest threat immediately after the clearance of natural vegetation since at this time vegetation cover is low but the soils have not yet had a chance to be degraded (and thus have their erodibility reduced) by inappropriate agricultural practices.

The results outlined above could be used in planning sustainable land use development. For example intensification of current landuse could be encouraged in resilient areas, i.e. those with low erosion in Figures 16 c and 16 d, in order to relieve the pressure of encroachment into less resilient regions. Furthermore, one philosophy for achieving sustainable development is to manage for the bad times rather than trying to determine a 'carrying capacity' in an environment that is subject to drought and therefore is not in equilibrium. The scenarios outlined above are 'bad times' scenarios. If an area does not erode under these conditions it is unlikely to be susceptible to soil erosion. If an area does erode under these conditions then it is an area where erosion control measures should be considered.

4.4.3 Deforestation Scenarios

It is easy to model the effect of complete deforestation of the lake catchment by simply running the model with zero vegetation cover. Figure 16f shows the results for the entire

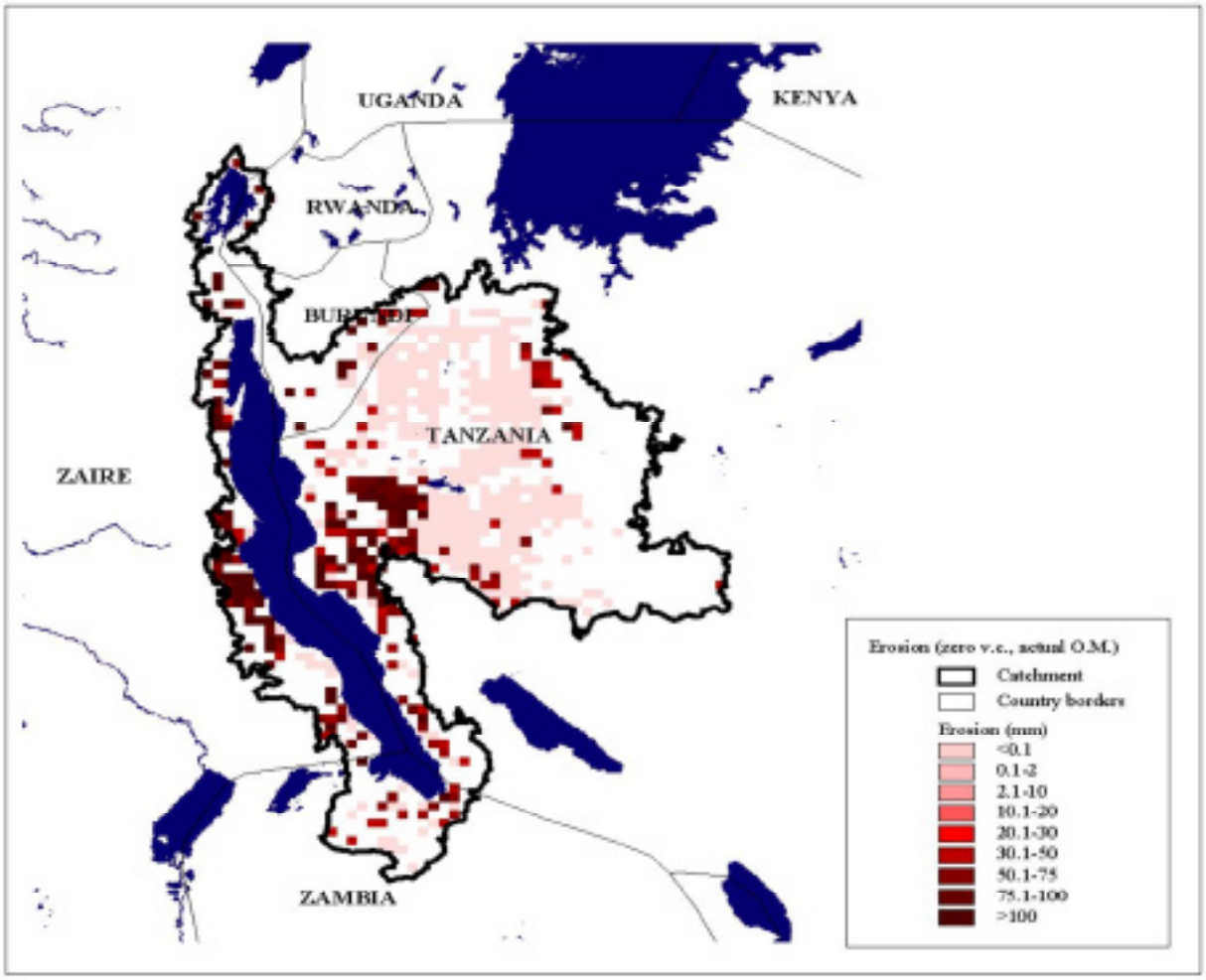

Figure 18. Deforestation erosion scenario. Only those areas that are currently forest are shown, in other areas erosion has been set to zero. Regions of high predicted erosion represent those areas of forest that will be most susceptible to erosion if they are cleared.

region, while figure 16e show the results for zero vegetation cover and less than 1% organic matter. Figure 17 shows the forest cover in the catchment while Figure 18 shows the results for zero cover and actual erodibility for those areas that are currently forest. All regions with a different landcover have been set to zero. This map can be used to provide an indication of those areas that are most susceptible to erosion if they were deforested. Clearly areas of potentially high erosion are those that should be given the highest priority for forestry protection.

Cohen *et al.,* (1993) noted that it is not just deforestation that is important in controlling sediment inputs into the lake but also catchment size (small catchments tend to have stronger linkages between what happens on the slopes, and subsequently in the river channels and the lake). The sediment delivery and routing technique that we have developed is a function of catchment size and slope, thus by routing the results of this scenario we can quantitatively consider the effect of catchment size on sediment delivery. The results of doing this are used to illustrate the routing technique outlined in section 4.5 below. These results provide an indication of where and how much a particular part of the lake will be affected by erosion if the vegetation was completely cleared.

4.5 Routing of Erosion for Estimation of Sediment Transport to Lake Tanganyika

Though it was only specified in the contract to apply the routing to the March 1996 data, we ended up using the routing algorithm in three different ways. Firstly, we applied the method to the deforestation scenario in order to consider the sensitivity of erosion to catchment size (Section 4.5.2). Secondly, we evaluated it using daily interpolated raingauge data for March 1996 (Section 4.5.3). Finally, we applied it to dekadal FEWS data in the real time demonstrator (Section 4.6).

4.5.1 Method Development

The process of soil erosion by water includes soil detachment, transport and deposition. Our erosion model only considers detachment by overland flow, not where the sediment will be transported or when and where it will be deposited. To estimate sediment input into the lake we have to consider these factors. The eroded soil can be divided into two parts, (i) sediment deposited within a catchment when the sediment concentration is higher than the transport capacity (e.g. when topography is flat), or (ii) sediment transported out of the catchment when the concentration of sediment in the overland flow is less than the transport capacity.

Sediment transport capacity can be calculated using models such as the European Soil-Erosion Model (EUROSEM), WEPP, and the sediment continuity equation (Kothyari *et al.* 1997). However, such methods require detailed climatic, hydrologic and soil data on fine time steps (hourly or less). Furthermore, WEPP and EUROSEM require more than 50 input parameters. Therefore, such models are not really suitable for regional scale modelling, particularly in Africa where input data are relatively sparse, and a simplified method needs to be developed.

When sediment moves through a catchment, the route is primarily controlled by topography. The effects of slope on sediment delivery can be used to decide on the drainage direction within the cell on the basis of the steepest descent (Figure 19).

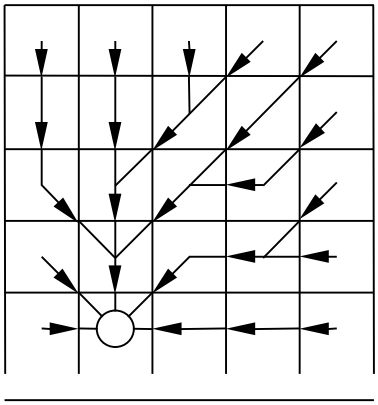

Figure 19. The sketch of sediment yield routing according to the steepest slope.

Such a routing approach can be readily implemented in the PC Raster software using dynamic modelling. Routed gross erosion (E_g) at the outlet of the catchment is:

$$E_g = \sum_{i=1}^{n} E_i \qquad (11)$$

where E_i is daily soil erosion. Pilotti and Bacchi (1997) routed erosion in this manner but it assumes that no deposition occurs. They justified this by quoting Foster and Meyer (1972) who found that the transport capacity of runoff from uniform slopes during moderate to intense storms is usually sufficient to transport all available soil if the slope exceeds 2 or 3 percent. This method can be implemented using the PC-Raster (Figure 20), however, it is very simplistic as not all of the eroded soil will be delivered to the outlet of a catchment that has a large flood plain or contains many swamps along its course for example. This is the case for many of the large rivers in the Lake Tanganyika catchment.

One way to incorporate deposition is to estimate the sediment delivery ratio(*Dr*), the ratio of sediment yield to erosion. The delivery ratio of each cell in a catchment can be computed based on the "upland theory" (Boyce 1975, ASCE 1982), which argues that steep headwater areas are the main sediment-producing zones of a basin and that sediment production per unit area decreases as average slope decreases with increasing basin size. Thus the delivery ratio can be considered a function of contributing area and catchment size. *Dr* tends to diminish with increasing basin size at roughly the same rate as the sediment yield per unit area (Richards 1993).

The routed derivery ratio (Dr_i') in *i*'th cell is controlled by the contributing area in the following manner:

$$Dr_i' = Dr_i.Dr_{i-1}.\, Dr_{i-2}\ldots Dr_{i-N} \qquad (12)$$

where n is the number of pixels in the up stream catchment. In addition a power relationship has been demonstrated between the delivery ratio (*Dr*) and catchment size (ASCE 1975):

$$Dr = C_3 A^{C_2} \qquad (13)$$

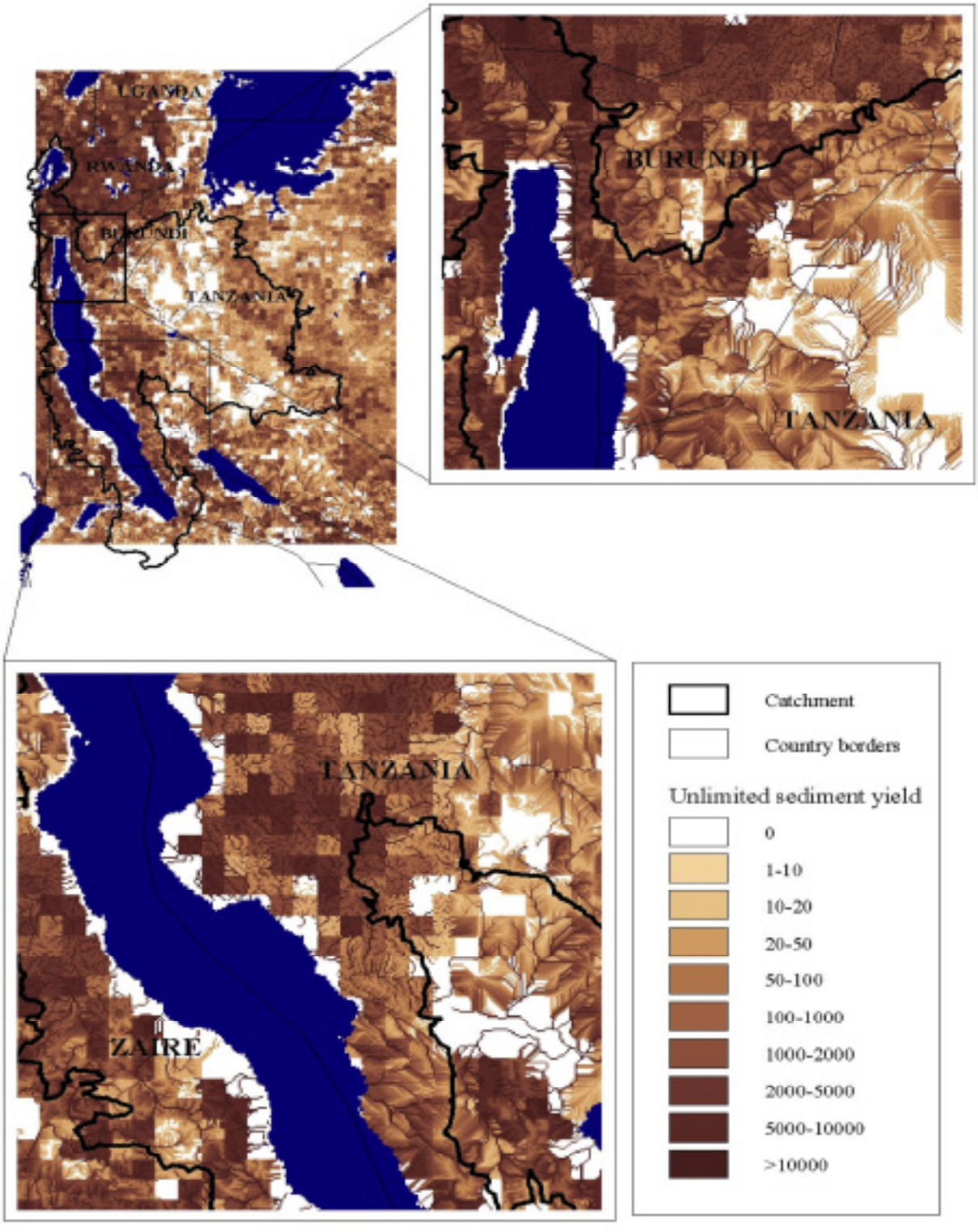

Figure 20. Estimate of sediment transport (mm/dekad) for the zero vegetation cover scenario assuming no deposition and routed according to the steepest slope.

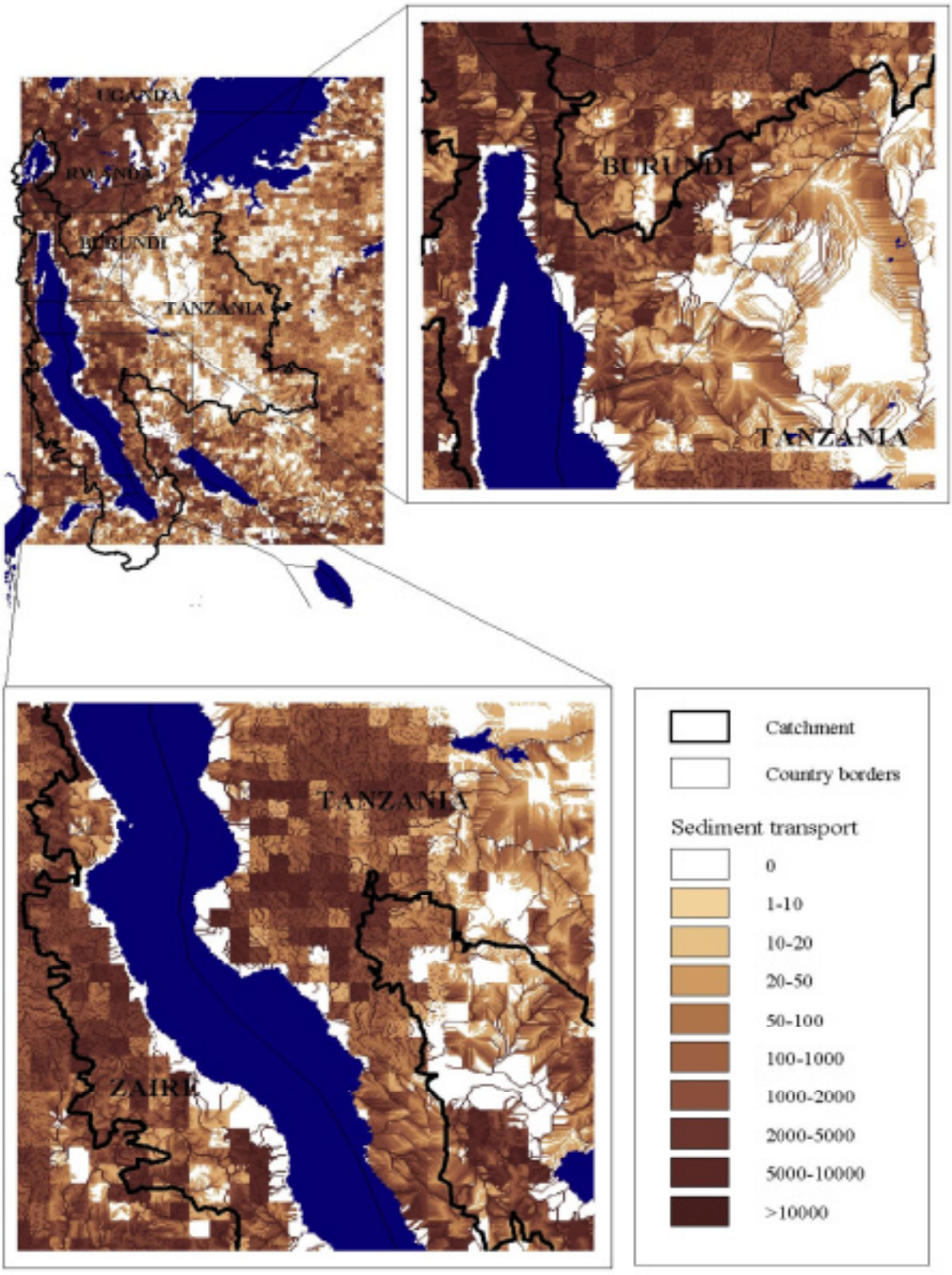

Figure 21. Sediment yield (mm/dekad) for the zero vegetation cover scenario estimated using the sediment delivery ratio and routed according to the steepest slope.

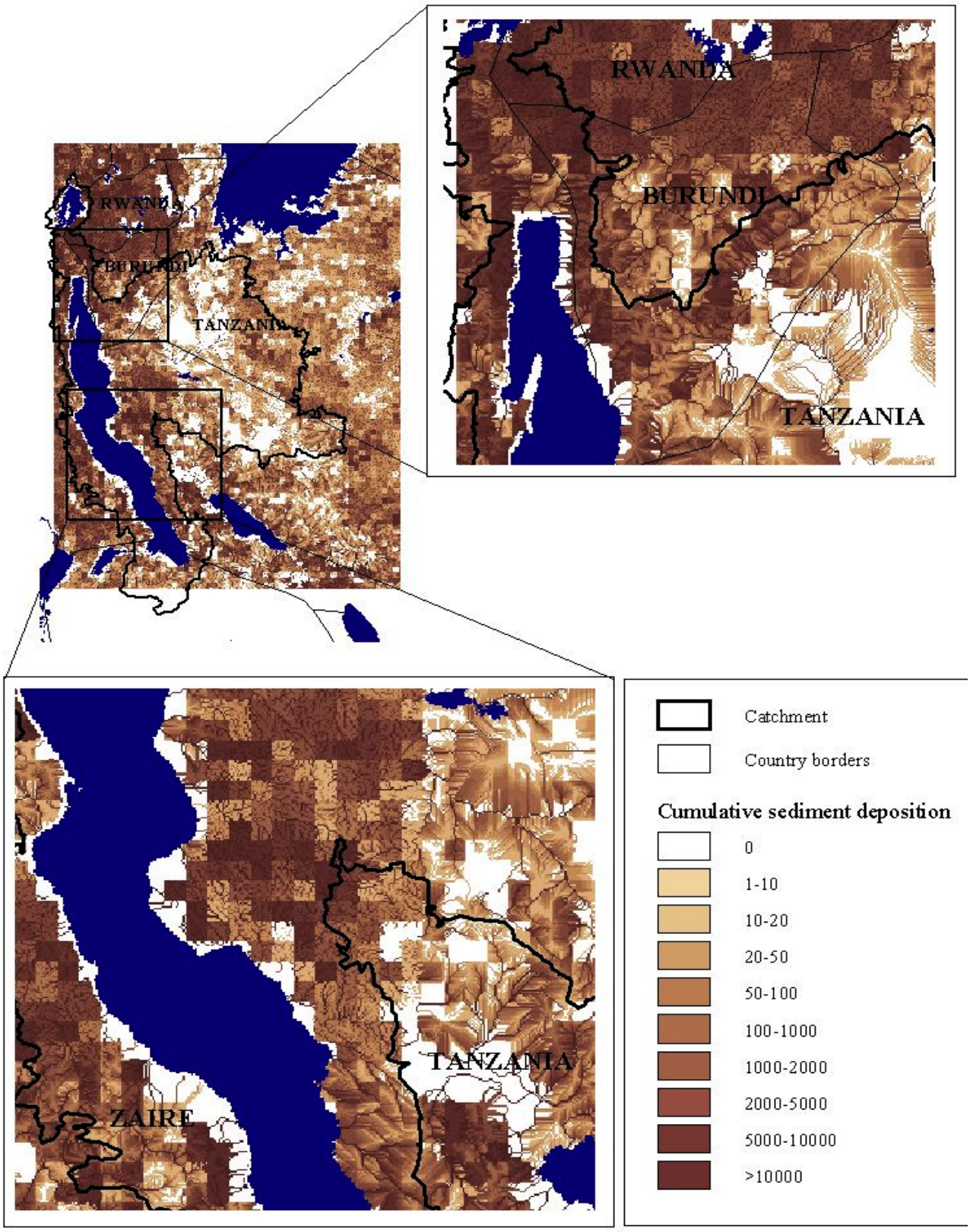

Figure 22. Sediment deposition (mm/dekad) for the zero vegetation cover scenario.

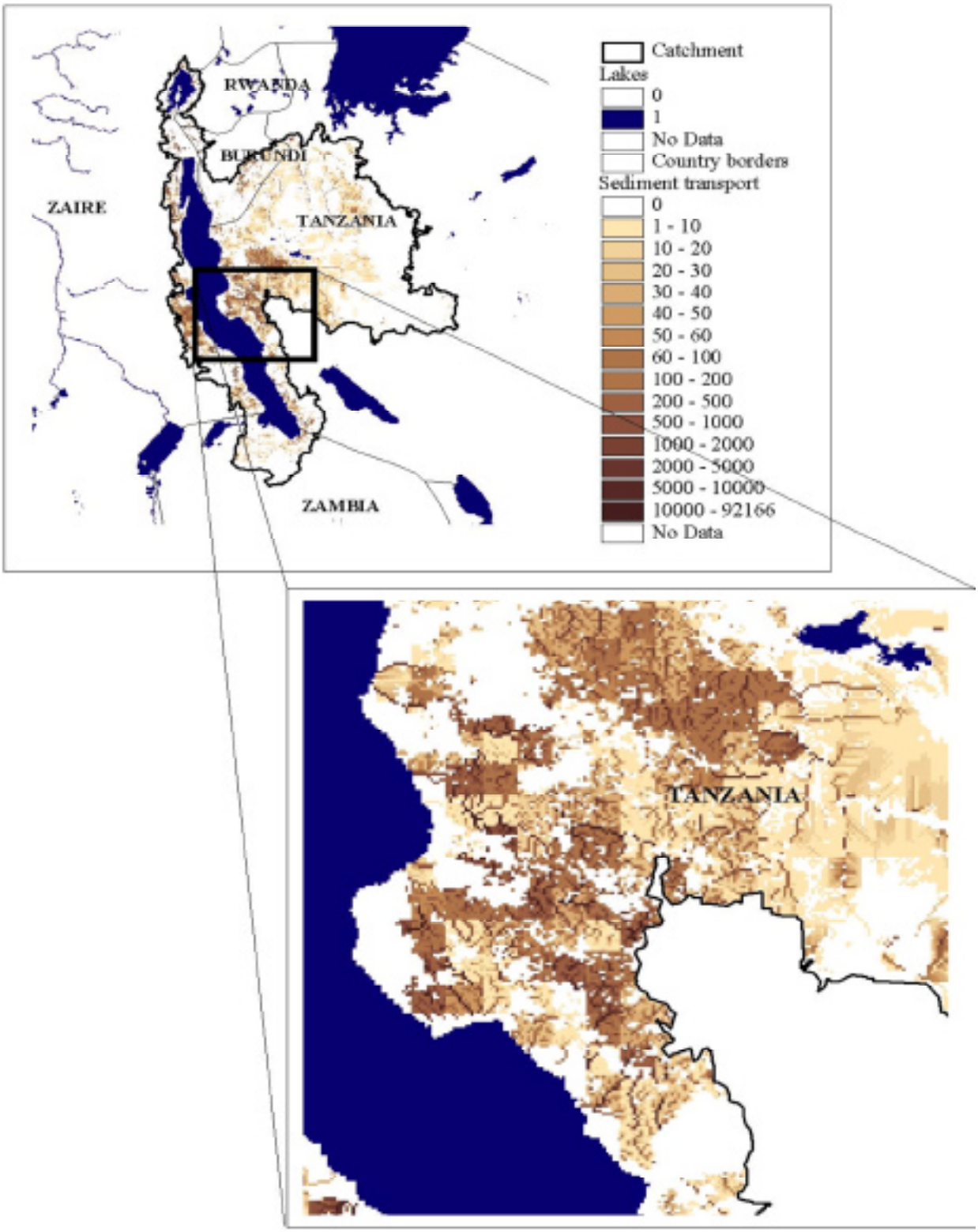

Figure 23. Map of erosion and sediment transport (mm/dekad) that would occur if regions of the catchment that are currently forest were deforested.

where C_2 and C_3 are empirical coefficients and A is the area of a catchment (km^2). This equation is applicable with C_2 = -0.125 in the USA (ASCE 1975), though the exponents are usually in the range between -0.01 and -0.25. There is less information available about the value of C_3, however, based on a set of catchments in the USA that were approximately 30 km^2, with a delivery ratio of approximately 30%, a value of C_3 of 0.46 was determined by Richards (1993) and this value is used here.

Therefore the routed delivery ratio in a raster image can be expressed as:

$$Dr_i' = C_3 \left(\sum_{j=1}^{i} A_j \right)^{C_2} \quad (14)$$

where i represents i^{th} cell, A_j is the cell size. The values of C_2 and C_3 outlined above were employed in this study. Once the delivery ratio is calculated the sediment yield E_y can be estimated using:

$$E_y = \sum_{i=1}^{n} Dr_i' E_i \quad (15)$$

where E_i is the soil erosion in i^{th} cell, and n is the number of cell upstream. Figure 21 shows the sediment yield estimated using the sediment delivery ratio and routing according to the steepest slope (equation 11) for the zero vegetation cover scenario.

The sediment deposited in each cell (E_d) is the soil erosion minus the transported sediment:

$$E_d = E_g - E_y \quad (16)$$

Figure 22 shows the estimated sediment deposition for the zero vegetation cover scenario.

4.5.2 Routing and Deforestation Scenario Results

Figure 23. Shows the map of erosion and sediment transport that would occur if regions that are currently forest were deforested. The results suggest that there are many areas of Democratic Republic of Congo and Tanzania located in the middle of the lake catchment that would be highly susceptible to erosion if they were deforested. These regions could be thought of as primary targets for forest protection measures.

4.5.3 Results of Sediment Routing for March 1996

We applied the sediment routing for March 1996 before we had finished the evaluation of the most appropriate method of rainfall estimation. We chose to use daily GTS plus BKTZ data because, in the absence of validation information, we thought that it was more physically realistic to route daily rather than dekadal erosion. However, it is clear from section 4.1 that GTS based rainfall, overland flow and erosion estimates are lower and less accurate than FEWS estimates, particularly in Democratic Republic of Congo. Thus erosion and sediment yield in Democratic Republic of Congo may be underestimated in the following analysis.

The maps of daily erosion (before routing) suggest that the total soil loss in March 1996 was 3.96×10^6 tonnes in all the catchments surrounded the Lake Tanganyika. The northern region of the Lake Tanganyika catchment centred on Rwanda and Burundi suffers severe erosion and is a likely source of lake sediments.

A

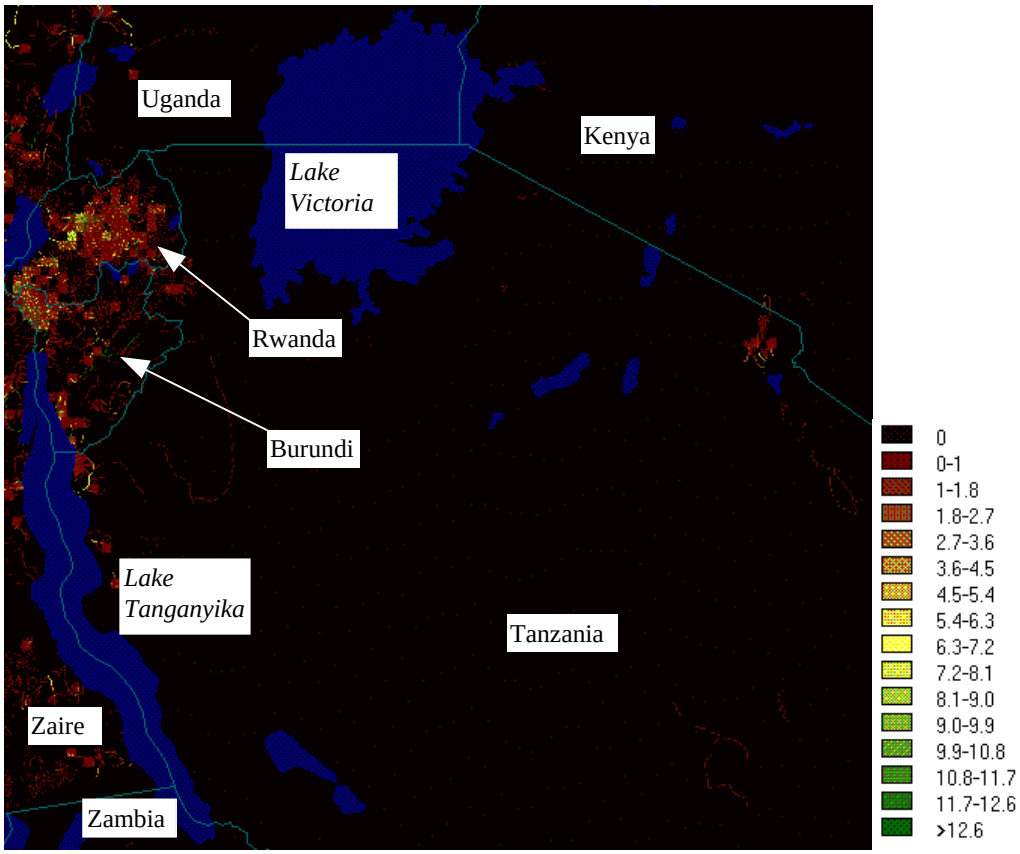

B

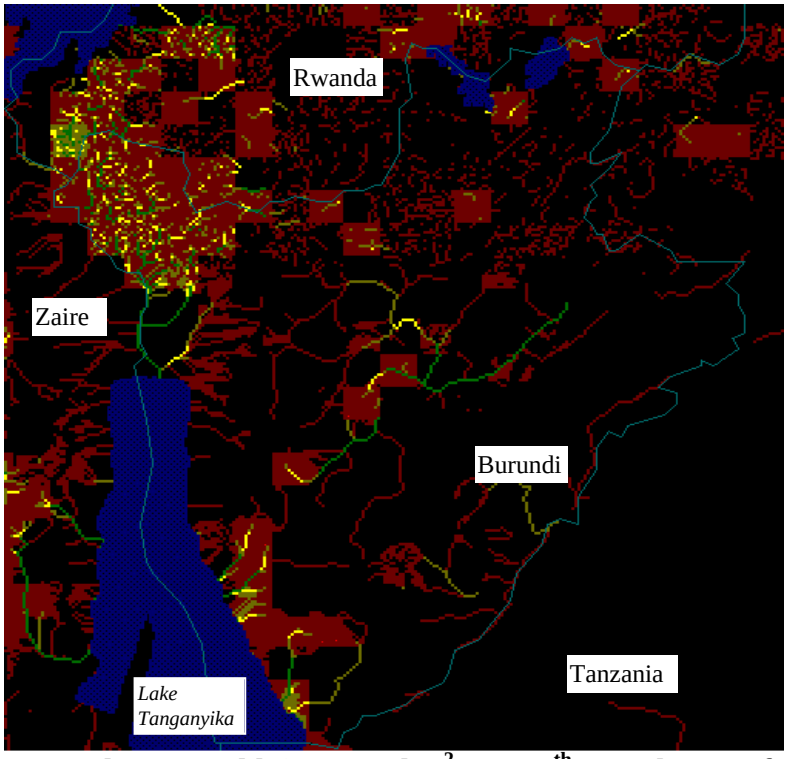

Figure 24. Sediment yield (x1000 t km^2) on 30th March 1996 for (A) the entire lake catchment, and (B) northern Lake Tanganyika, the site of most severe erosion.

A

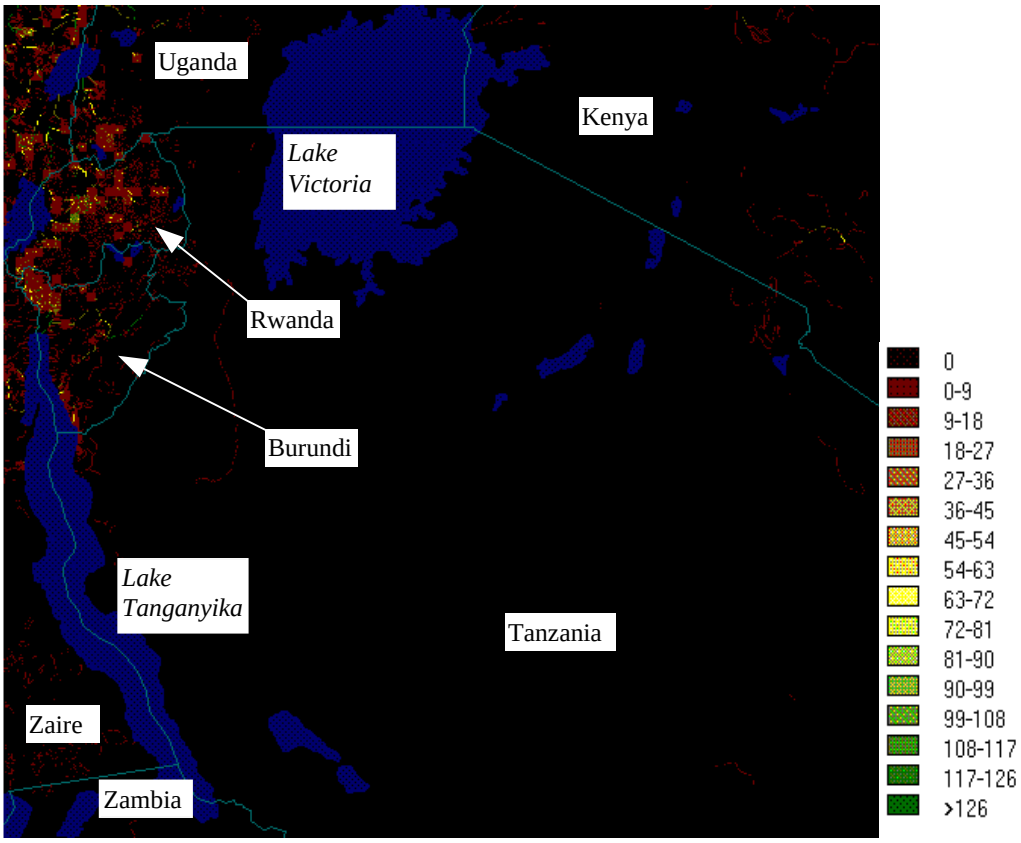

B

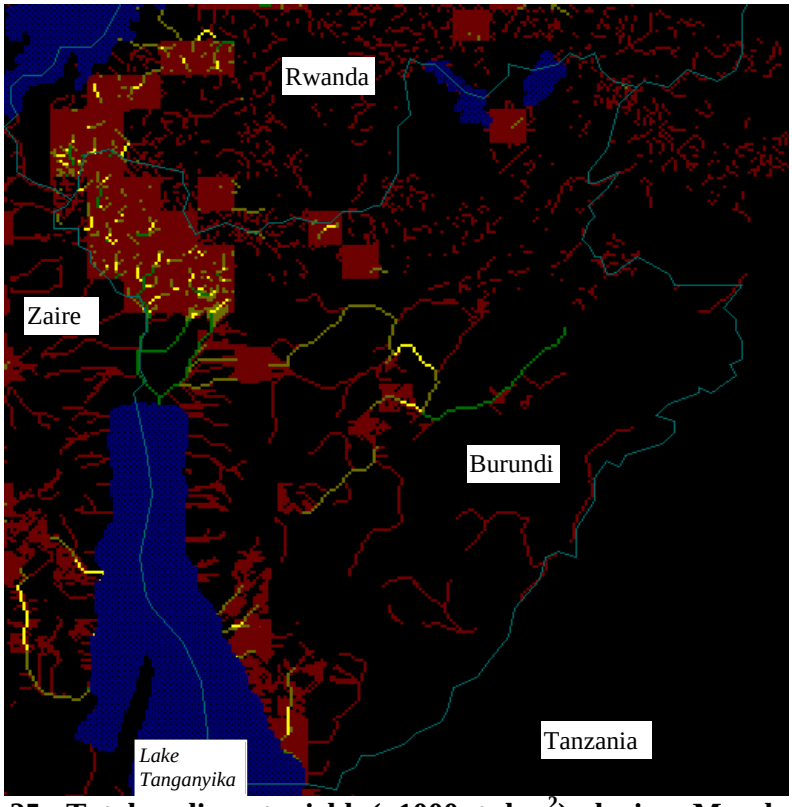

Figure 25. Total sediment yield (×1000 t km^2) during March 1996. A) The lake catchment, B) northern Lake Tanganyika.

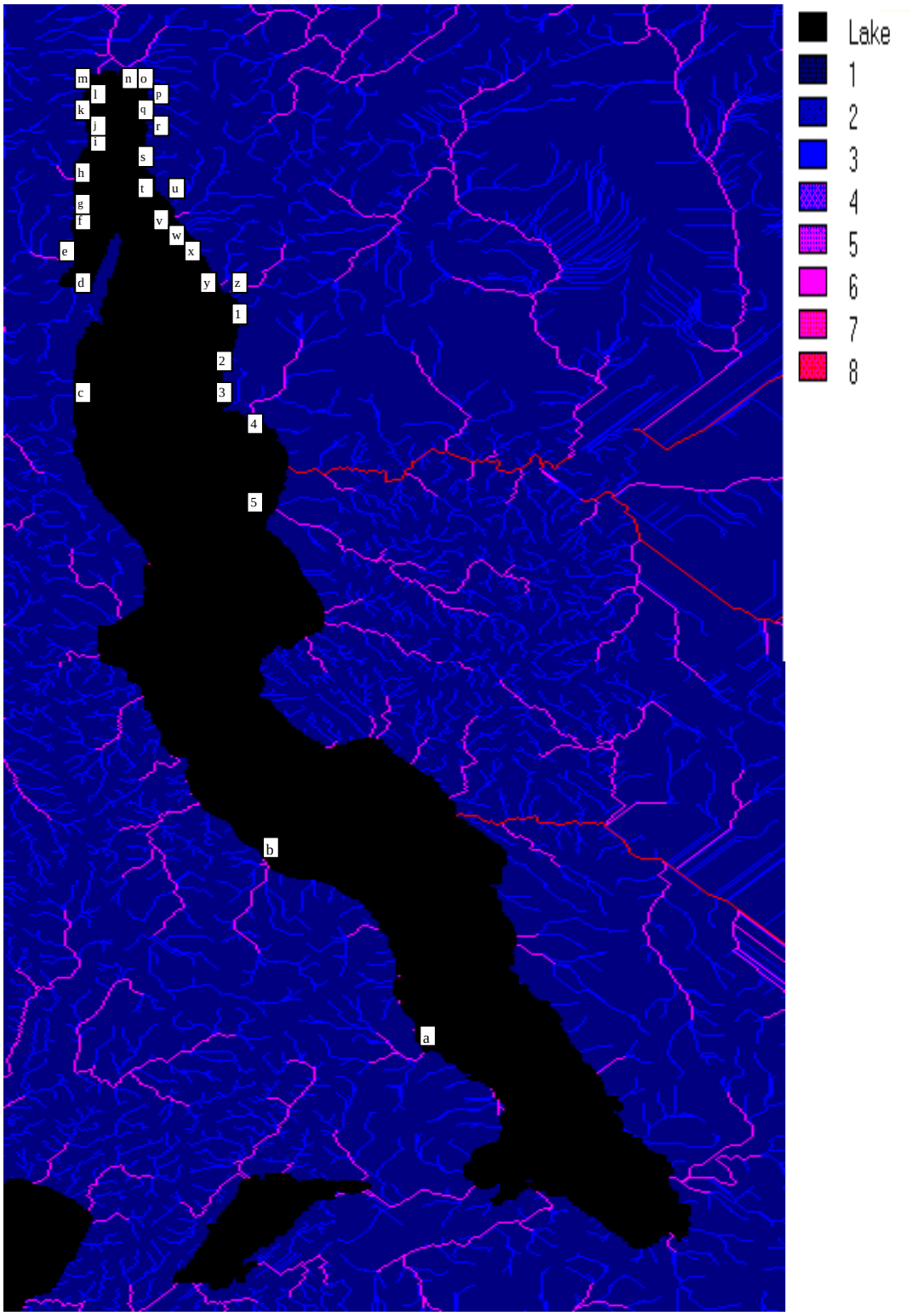

Figure 26. Channel network in Tanzania. The letters and numbers represent the rivers that transported sediment into the Lake Tanganyika during March 1996.

The results for the day with the highest erosion are shown in Figure 24, while those for the entire month are shown in Figure 25. At the scale shown in Figure 24a the reader gets a picture of the erosion prone areas, however, the fine detail of the channel network can not be seen. Figure 24b is zoomed in on the region of Rwanda, Burundi and eastern Democratic Republic of Congo that shows the highest amounts of sediment transport to the lake on this day. This figure depicts both hillslope and channel sediment transport. The contiguous regions that are not black are areas of high hillslope erosion and the networks overlying and surrounding these blocks are areas where sediments transported from the hillslopes concentrates in river channels.

Routing estimates that the total amount of sediment reaching Lake Tanganyika during the month of March 1996 was around 1.6×10^6 tonnes (Figure 25), while sediment deposited in the catchments around the Lake Tanganyika was around 2.4×10^6 tonnes. The main source region of sediment to the lake appears to be Burundi, and to a lesser extent Democratic Republic of Congo. In order to consider the yield of individual rivers the channel network and stream order extracted from the 1km DEM is shown in Figure 26. We do not have detailed enough maps to refer to most of the rivers by name so we have assigned them letters and numbers. The amount of sediment reaching the mouth of these rivers is shown in Appendix 2 table 1. To summarise this data, the sub-catchments that feed into the river Rusizi (river n in Figure 26) provide 63.6 % of the sediment yield into the lake (Figure 25a and 25b). Most of this sediment yield was generated in the rainfall events on March 7th, 20th, and 30th with 16.8%, 20.6% and 24.8% respectively (Appendix 2, Table 1).

It is interesting to note that the region of highest sediment yield in Figure 16b is the same region that is cloud covered throughout March (Figure 3), so vegetation cover in this region was averaged from the preceding and following months. These regions will tend to suffer high overland flow and erosion because it is raining for much of the time, however, they are also the places where the actual vegetation cover is at its most uncertain and thus the sediment yield results should be treated with caution. This highlights a paradox when using remote sensing to estimate both rainfall and vegetation cover from visible and IR remote sensing. When it is actually raining, and erosion is occurring, remote estimation of vegetation cover is not possible via optical and near infrared methods.

4.6 Real Time Erosion Modelling Demonstrator

The erosion model and sediment routing methods outlined above have been implemented using AVHRR LAC imagery, obtained from the Kigoma station, for one month in order to illustrate how the model can be run on an operational basis using locally based equipment and personnel. This provides NDVI at a finer spatial resolution than ARTEMIS data (1km NDVI), and potentially in near real-time.

This 1km spatial resolution NDVI data should allow us to provide a more accurate erosion estimate because the scale at which the model is applied affects the accuracy of the results (Drake *et al.*, 1999). As the spatial resolution is increased, predicted erosion increases. However, at 1km spatial resolution we have still averaged out much spatial variability. To overcome this problem we have implemented the Polya function as previously stated (See Appendix 1 for an outline and validation of the method). This technique uses eight neighbouring pixels to estimate the sub-pixel histogram at a specified spatial resolution (we use 30 meters), thus the output of the Poyla function is an image with a degraded spatial resolution (8km) that contains a histogram for each pixel. The erosion model is then be run

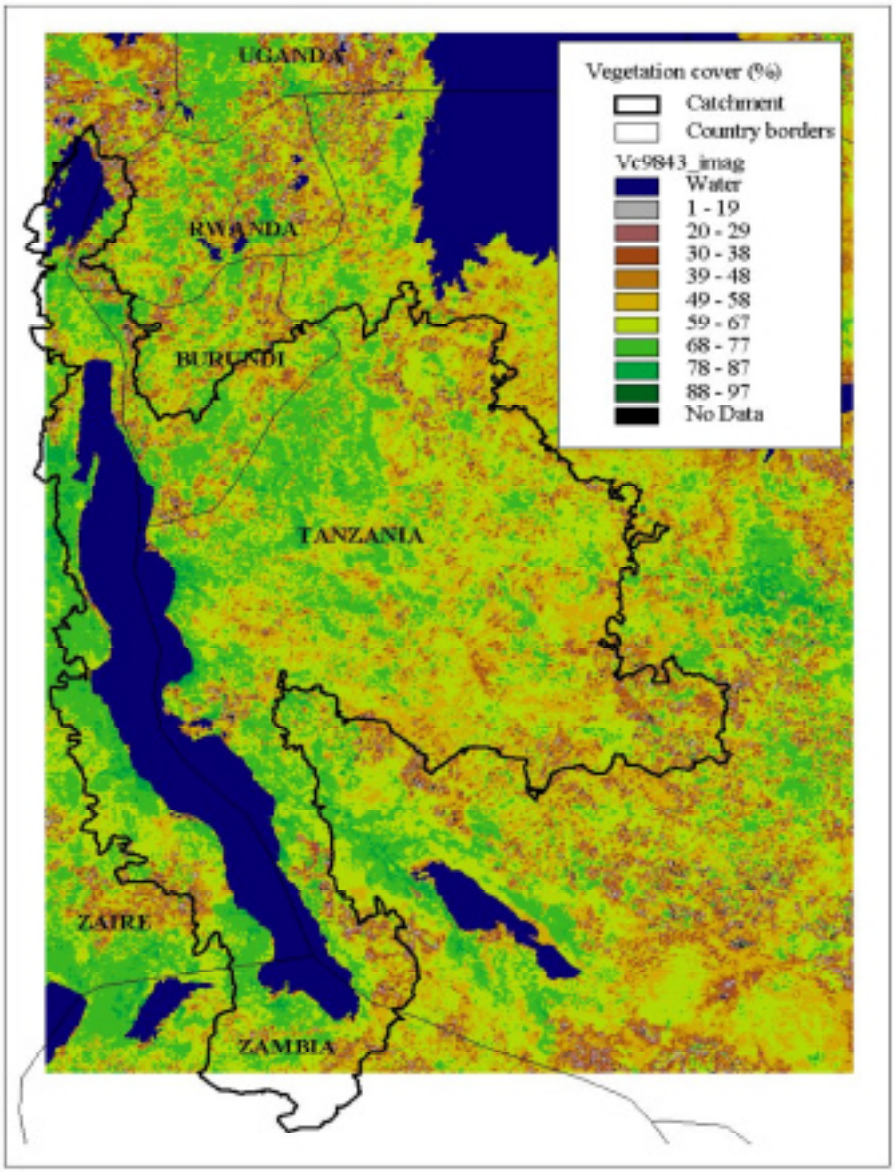

Figure 27. Vegetation cover image (1 km NDVI) for April 1998. Data from the March and May were used to fill the gaps in areas of persistent cloud cover.

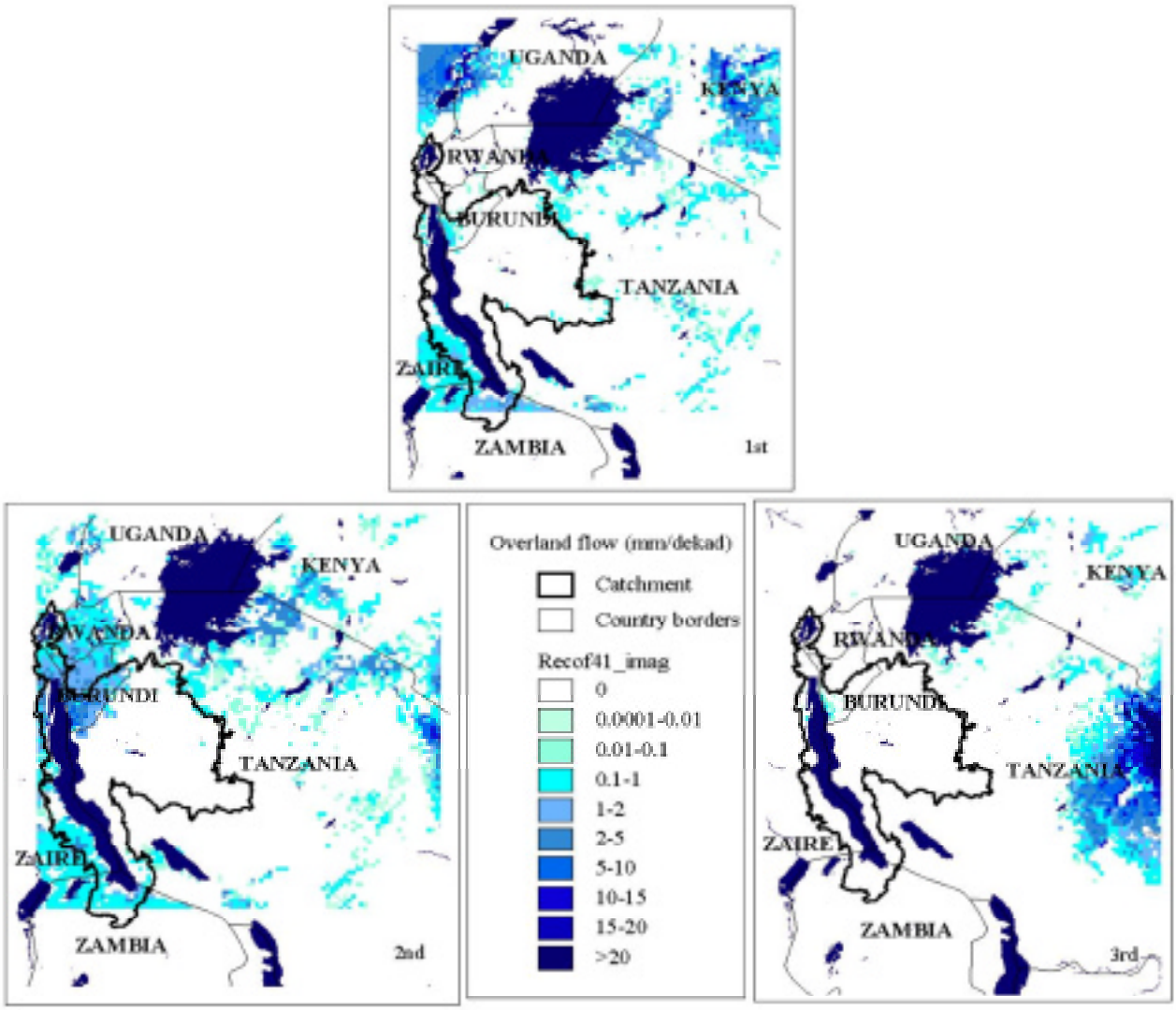

Figure 28. Overland flow for the three decads of April 1998.

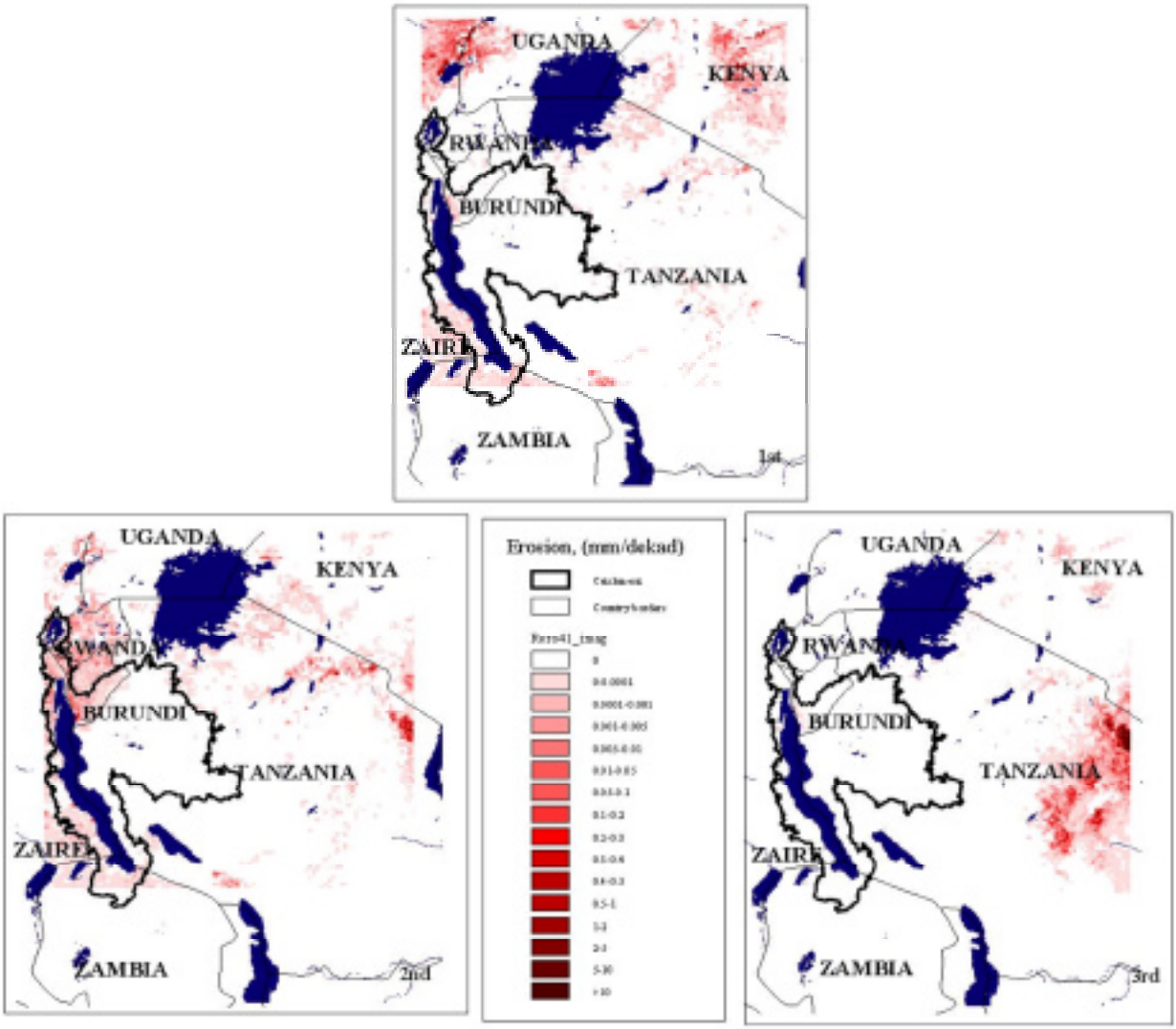

Figure 29. Erosion for the three decads of April 1998.

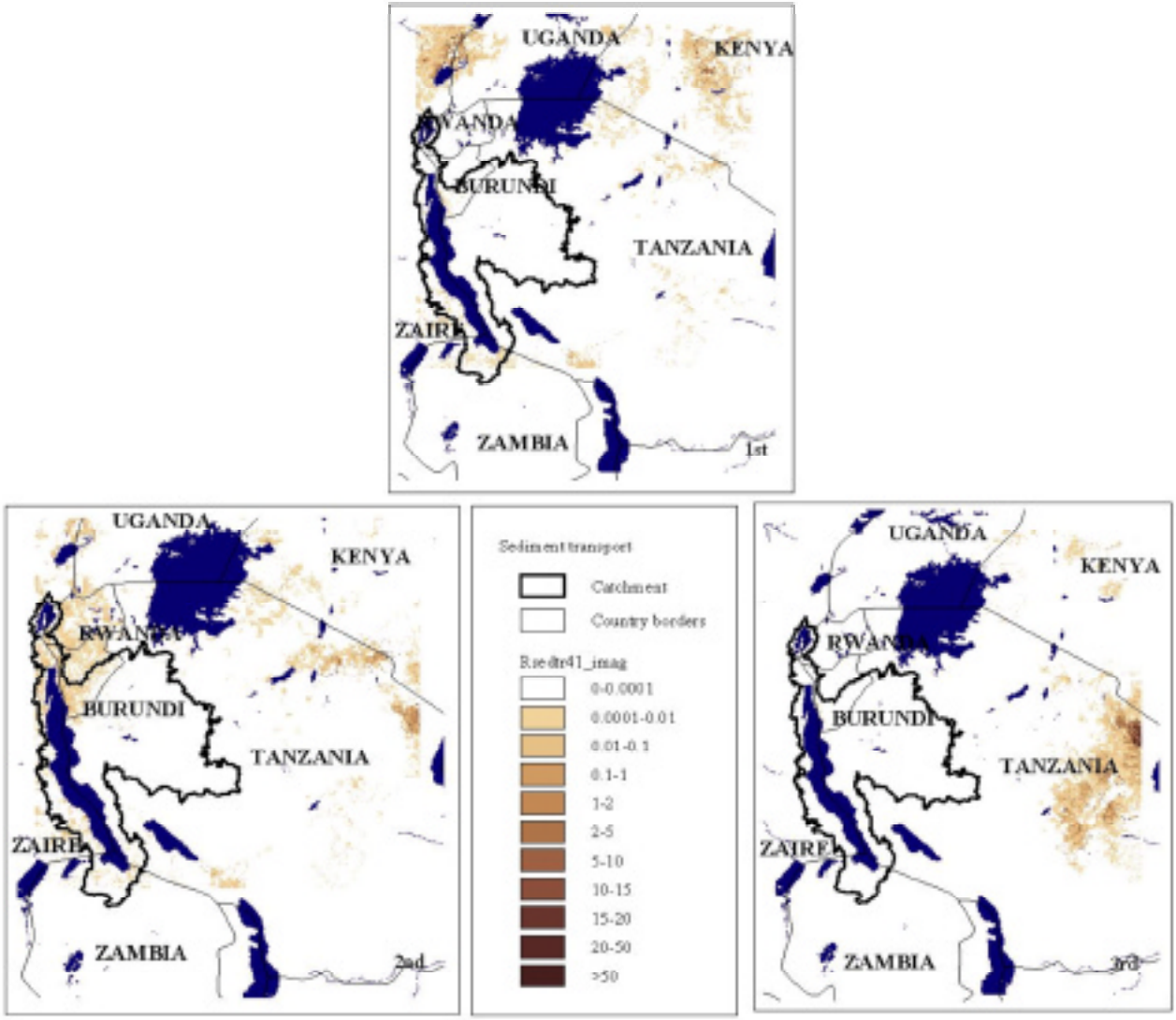

Figure 30. Sediment yield for the three decads of April 1998.

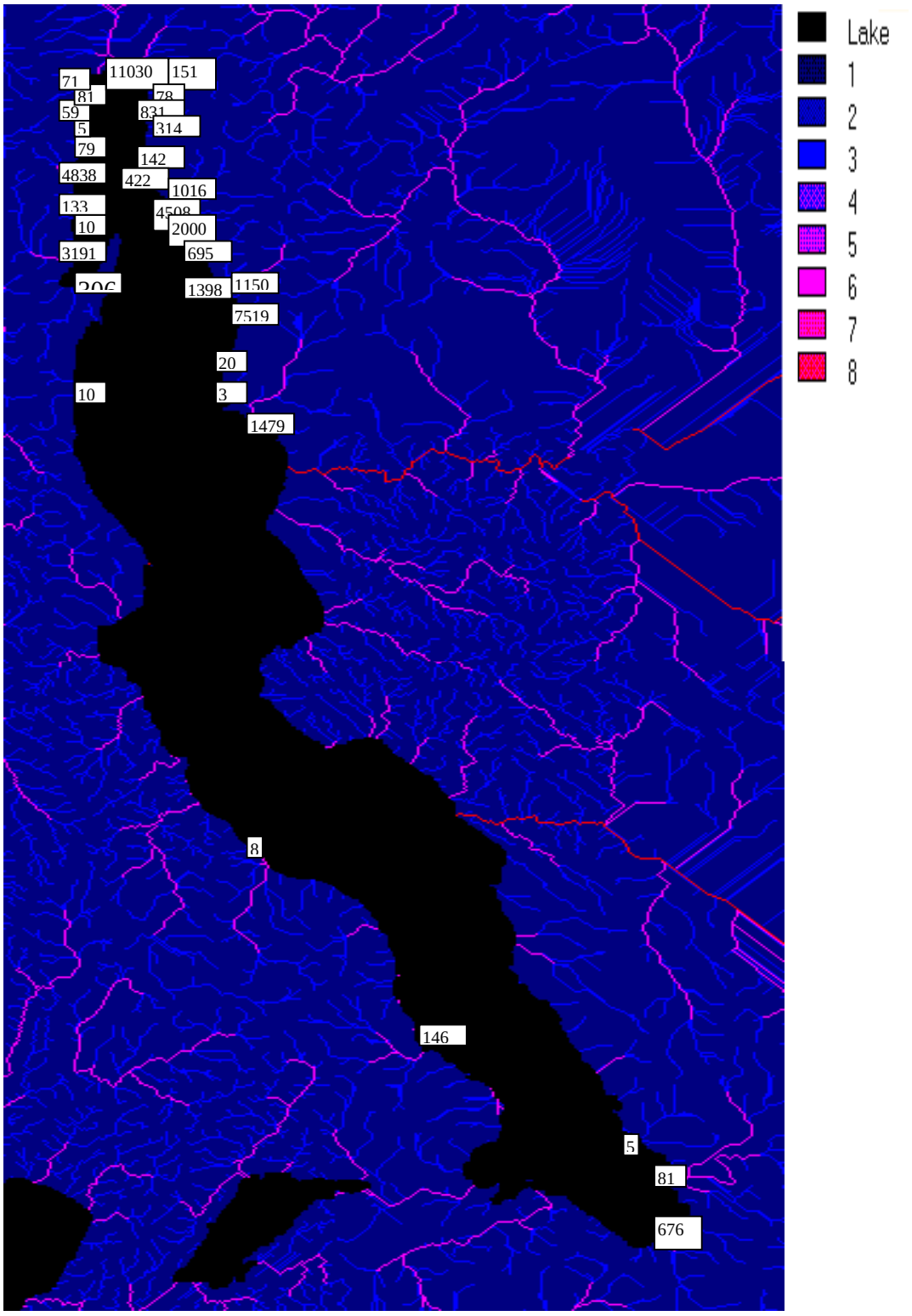

Figure 31 Total sediment yield to lake (tonnes) for April 1998.

for each column of the histogram and the results summed to obtain erosion for the dekad in question.

AVHRR data was obtained from the Kigoma receiving station for 1997 and 1998. We applied the model for the wettest month in the 1998 wet season (April 1998). The AVHRR LAC archive from Kigoma typically provided two daytime images a week, this being the number that were judged to be relatively free from cloud. However, because of the adverse weather conditions cloud was still a problem and the maximum value composite for April contained many gaps where cloud cover was present for the entire month. To overcome this images from the March and May were used to fill the gaps. The resulting vegetation cover image is shown in Figure 27. Though there are few areas of low cover (<20%) at this time of year there are significant areas of intermediate cover (20-40%). The erosion model was implemented for the three Dekads of April using these NDVI data, FEWS rainfall estimates, estimation of the number of rain days from indicator kriging of GTS data, and the slope and K maps produced earlier.

Figure 28 shows the overland flow, while Figure 29 shows the resultant erosion. Unlike March 1996 there is a considerable amount of rainfall throughout much of the region in April 1998. However, only in the second dekad is there substantial rainfall, overland flow and erosion in the Lake Tanganyika catchment itself. The model predicts less erosion in April 1998 than in March 1996, however, in general it is found in the same places as in March 1996. The reason for this difference in sediment yield is not clear. It may be because the vegetation cover in April 1998 was considerably higher than in March 1996. This increase in vegetation cover can be attributed to the extremely high rainfall experienced during the 1998 wet season, attributed to the El Nino conditions of that year.

Figure 30 shows the total monthly sediment transport results for the Lake Tanganyika region for the three dekads of April 1998. In order to consider the yield of individual rivers the amount of sediment reaching the mouths of these rivers was calculated. Forty three rivers produced significant sediment inputs into the lake during April with the vast majority occurring in the second dekad. The total sediment yield of these rivers is shown in Figure 31 while the results are tabulated in the Appendix. However, a summary of the results is provided here. The main source regions of sediment to the lake appear to be located in parts of Burundi and to a lesser extent Democratic Republic of Congo. As was found in March 1996, the Burundi sub-catchments of the river Rusizi provides the most sediment. However, in April 1998 they only provide 17% of the total sediment yield, whereas in March 1996 this region provided 60%. High erosion in this catchment can be attributed to relatively steep slopes (0.64 m/m, or 33%), high overland flow (4 mm), and most importantly low vegetation cover (7%).

4.6.1 Problems with Estimating the Sediment Delivery Ratio

Though the model appears to work quite well when routing sediment into Lake Tanganyika, it suggests that very little sediment reaches Lake Victoria. However, it is known that sediment does reach this lake and his seems to illustrate a deficiency in the model when it is applied to large catchments that contain a considerable amount of flood plain. Once a catchment reaches a certain size then sediment yield seems to abruptly cease. At the moment we are not certain why this occurs but it could be because the constants used in equation 11 were derived by studying small catchments and are not directly applicable to larger ones.

Further limitations of the technique are that the sediment delivery ratio is a 'black box' concept that lumps together and fudges a wide range of hillslope and channel processes. Changes in the rates of these different processes can cause delivery ratios to vary from year to year as annual rainfall and runoff vary (Walling 1983, Richards 1993). Furthermore, different methods of estimation in the field produce different results (Walling 1983) so the accuracy of the routing method we have developed is, in fact, almost impossible to validate.

Calculation of transport capacity provides a more physically based method for modelling sediment deposition. However, the sediment delivery ratio method we have developed here fits well with the requirement to route sediments on a daily or dekadal basis. Transport capacity cannot be easily calculating using such a coarse timestep. Thus improvements in estimating sediment delivery require improvements in the timestep of the routing algorithm. This would also make the model more plausible since, at present, we assume that all the sediments that enter the lake are transported and deposited in a single event once every 10 days.

5. Conclusions

The results of the retrospective feasibility study and the real time demonstrator show that regional scale erosion modelling can provide a general picture of the source areas of erosion in the Lake Tanganyika catchment, and estimates of the quantity of sediment transported into the lake. Previous spatial studies of lake sediment inputs have relied on the interpretation of satellite imagery (and topographic maps) to simply assess the amount of forest in a catchment, in order to determine those catchments most likely to provide increased sedimentation due to deforestation (Cohen *et al.*, 1993). The model presented here provides a more direct method for estimating sediment affected areas of the lake, supplies maps of the source areas, and thus provides a significant improvement in our spatial and temporal understanding of the pollutant that provides the most immediate and significant threat to the lake ecosystem. Furthermore, if real time monitoring were implemented on an operational basis, the model has the potential to provide the riparian nations with up to date information on erosion and sediment yield that could be used to target further research and co-ordinate remediation measures.

The model has also been used to assess the sensitivity of the catchment to erosion and to model scenarios that have allowed for an appraisal of the potential effects of land degradation and deforestation. Large parts of the catchment have low slope and thus produce little erosion. Erosion is largely restricted to the mountainous regions, however, not all mountains produce erosion, presumably because some possess high vegetation cover. The results suggest that there are a few key regions in Burundi, Democratic Republic of Congo and Tanzania that are prone to erosion. Some of these regions have already been deforested and degraded (i.e. Burundi) and seem to be producing significant sediment input to the lake. In these areas the model suggests alleviation measures are required. Other erosion-prone areas have not yet been deforested, but if they were the model suggests they would also produce significant lake sediment input. These regions are prime targets for any forest conservation measures that might be considered, and as such are outlined in Figure 32. Region 1 (centred on Burundi) provides significant erosion and sediment yield for all the different aspects of this study. Region 3 (in Democratic Republic of Congo), erodes under all conditions investigated here but does not provide as much erosion or sediment inputs to the lake as Region 1. Region 2 (in Tanzania) is sensitive to erosion, deforestation and land degradation. Furthermore, significant erosion is predicted in March 1996 but only in restricted areas as there is much forest left in the region.

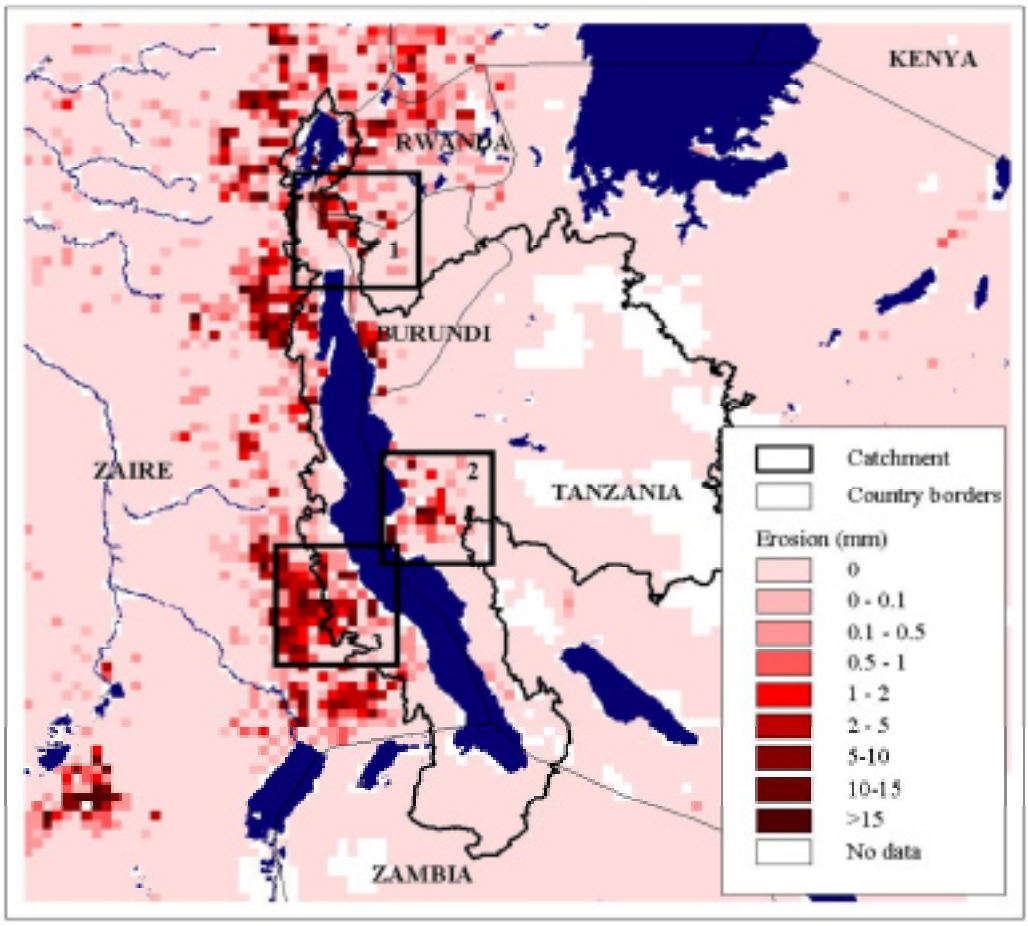

Figure 32. Regions that the results of this study suggest are most sensitive to erosion and require further study.

However, many of the model results should be treated with caution. The coarse resolution of the data only allows a general assessment of the problem to be made and remediation measures such as terracing or small scale agro-forestry systems, cannot be resolved at this scale. Thus it is not possible to assess the effects of such measures using a model implemented at the scale considered here. Furthermore, the true accuracy and precision of the model, and of many of the input parameters, has not been assessed. One of the most likely sources of inaccuracy is associated with the use of NDVI to estimate vegetation cover. Vegetation cover is the most sensitive parameter of the model and is thus the most important parameter to estimate correctly. Total vegetation cover estimates are needed, however, NDVI is most sensitive to green vegetation cover and thus may underestimate cover when there is a large amount of dead, and/or senescent material on the ground or in the canopy. This will lead to an over-prediction of erosion. Furthermore, NDVI estimates cannot be obtained during cloudy periods, and are depressed by partial cloud cover. Atmospheric effects can also affect the result, though these are partly taken into account by the empirical NDVI – vegetation cover relationship we derived using only the satellite-based measurements. All these effects will reduce predicted vegetation cover and it is thus possible that some areas of low predicted cover may be due to persistent sub-pixel cloud. This problem would manifest itself most in mountainous regions, where in the wet season cloud may develop over the peaks of the highest mountains on a daily basis.

Because of these problems no estimates of the accuracy of the model results can yet be provided and we would be reluctant to use solely these model results to identify the areas most at risk. Field work and/or higher spatial resolution studies in the regions that these results suggest are most sensitive to erosion are needed to confirm the findings of this study. Furthermore, improvements in the model parameterisation using sensors such as SeaWiFS, and MODIS would help improve the model implementation as discussed below.

6. Further Work

Because of the limitations provided by the coarse resolution of the model, it would be most effectively used if it formed part of a more complex, multi-scale modelling package. Ideally we envisage a system whereby the coarse spatial resolution model is implemented in order to provide a general picture of areas that are responsible for large amounts of sediment input to the lake. Erosion prone areas are then targeted by high-resolution sensors, such as the Landsat Thematic Mapper (TM), in association with limited fieldwork, in order to parameterise more detailed models to: (i) provide a more detailed assessment, (ii) confirm coarse resolution model predictions, and (iii) to study the effects of any erosion alleviation measures that might be implemented.

This research has also highlighted numerous avenues of possible further research in terms of the development of the regional soil erosion model. With regard to of ease of operation, the most time consuming aspect of running the model on an operational basis is the daily interpolation of the GTS data using indicator kriging in order to derive the number of rain days per dekad. This problem could be eased if we estimated rain days from METEOSAT-derived data and imagery, a relatively simple methodology but one currently unimplemented. Such a methodology might also provide rainfall maps with more spatial detail. Methods for estimating rain days from CCD data have been developed and could be readily validated using both the GTS and the independent raingauge data. We are investigating this possibility as part of the PhD research of Elias Symeonakis.

However, if the model was run on a daily basis, estimates of actual rain days would not be needed. Recent developments in United States rainfall prediction from geostationary satellites claim to be able to predict rainfall on an hourly basis, however implementation of the method requires an initial calibration of the satellite-derived data using rainfall radars, and there are few suitable in Africa.

One of the weaker aspects of the model is the sediment yield estimation. The equation we have developed relies on an empirical relationship between catchment size and the sediment delivery ratio. This could be improved through efforts to model the overland flow and erosion hydraulics rather than relying on empirical relationships, and by comparison of the method with data collected in the field.

A further way of estimating lake sediment inputs is to try to directly detect sediment plumes in the lake using satellite imagery. We currently have a Masters student investigating this possibility and final results will be available in September. Early results indicate that large plumes are indeed visible in the data from high spectral resolution, low spatial resolution sensors, though it remains to be determined whether such plumes can be observed using AVHRR. Data from the high spectral resolution (ATSR) instrument is, in fact, available on a near real-time basis via the European Space Agency NRT ATSR system, and so would be suitable for use in a long-term monitoring system.

In terms of vegetation cover there are numerous potential methods for improving this estimate. Total vegetation cover is closley related to optical reflectance, but not so well related to infrared reflectance, and this limits the utility of NDVI estimates. Because SeaWiFS has numerous optical channels it is a prime candidate sensor for measuring total vegetation cover at a regional scale. MODIS will also be good in this regard and will provide a higher spatial resolution (250 m) than either SeaWiFS or AVHRR. In order to get more accurate estimates of cover we also need to move away from vegetation indices and investigate techniques such as mixture modelling that have been shown to be more accurate, albeit currently only at the Landsat TM scale.

Certain aspects of model development will become very easy once the MODIS global data archive becomes available in 14 months time. With MODIS data products we could improve the overland flow estimates by using the evapotranspiration product, look at the effect of fire on erosion using the fire product, examine the effect of landuse change on erosion using the landuse change product, and investigate improved estimates of vegetation cover using the numerous vegetation products planned to be produced. In a similar way to that already observed with ATSR, MODIS will also allow direct detection of the sediment plumes within the lake itself. Such a capability will offer a unique synergy between erosion modelling and eroded sediment detection and these methodologies could be applied on a routine basis to support sustainable and ecologically sound development of the lake catchment.

7. References

American Society of Civil Engineers (ASCE) 1975. Sedimentation Engineering. Am. Soc. Civ. Eng., *Manuals and Reports on Engineering Practice*, No 54. Am. Soc. Civ. Eng., New York.

American Society of Civil Engineers (ASCE) 1982. Relation ship between morphology of small streams and sediment yield. *Journ. Hydraul. Div*. Am. Soc. Civ. Eng., **108**:1328-1365.

Arkin, P.A. and Meisner, B.N., 1987, The relationship between large-scale convective rainfall and cold cloud over the Western Hemisphere during 1982-84. *Monthly Weather Review*, **115**, 51-74.

Bailey, T. C. and Gatrell, A. C., 1995, Interactive Spatial Data Analysis. Longman.

Barancourt, C., Creutin, J.D. and Rivoirard, J., 1992, A method for delineating and estimating rainfall fields. *Water Resources Research*, **28**, 4, 1133-1144.

Boyce, R.C. 1975. Sediment routing with sediment-delivery ratios. In *present and Prospective Technology for Predicting Sediment Yields and Sources*, US Dept. Agric., Publ. ARS-S-40, 61-65.

Cohen, A.S., Bills, R., Cocquyt, C.Z., and Caijon, A.G., (1993) The impact of sediment pollution on Biodiversity in Lake Tanganyika, Conservation Biology, 667-677.

Drake, N.A. Vafeidis, A. Wainwright, J. and Zhang, X., (1995) Modelling soil erosion using remote sensing and GIS techniques, Proceedings of RSS 95 Remote Sensing in Action, 11-14 September 1995, Southampton, 217-224.

Drake N.A., Zhang X., Berkhout E., Bonifacio R., Grimes D., Wainwright J., Mulligan M. (Accepted 1998) Modelling Soil Erosion at Global and Regional Scales Using Remote Sensing and GIS Techniques, in Atkinson, P (eds.) Spatial Analysis for Remote Sensing and GIS, Wiley, London.

Foster, G.R. and Meyer, L.D. 1972. Transport of soil particles by shallow flow. *Transactions of the ASAE*, **15**(1):99-102.

Herman, A., Kumar, V.B., Arkin, P.A. and Kousky, J.V., 1997, Objectively determined 10-day African rainfall estimates created for famine early warning systems. *International Journal of Remote Sensing*, **18**, 10, 2147-2159.

Julien, P.Y. and Tanago, M.G.D. 1991. Spatially varied soil erosion under different climates. *Hydrological Sciences-Journal*, **36**(6):511-524.

Kothyari, U.C. and Jain, S.K. 1997. Sediment yield estimation using GIS. *Hydrological Sciences-Journal*, **42**(6):833-843.

Kothyari, U.C., Tiwari, A.K. and Singh, R. 1997. Estimation of temporal variation of sediment yield from small catchments through the kinematic method. *Journal of Hydrology*, **203**:39-57.

Maner, S.B. 1958. Factors affecting sediment delivery ratio in the Red Hill physiographic area. Trans. AGU, **39**(4):669-675.

Mitchel, J.K. and Bubenzer, G.D., 1980. Chapter 2: Soil Loss Estimation. In Kirkby, M.J. and Morgan, R.P.C., (eds), Soil Erosion, John Wiley & Sons, pp.17-62.

Patterson, G. G. and Makin, J. (Ed.) (1998) The state of Biodiversity in Lake Tanganyika – A Literature Review. Chatham, UK: Natural Resources Institute.

Pilotti, M. and Bacchi, B. 1997. Distributed evaluation of the contribution of soil erosion to the sediment yield from a watershed. *Earth Surface Processes and Landforms*, **22**:1239-1251.

Rawls, W.J., Ahuja, L.R., Brakensiek, D.L. and Shirmohammadi, A., 1993, Infiltration and soil Water movement. In: Maidment, D.R. (ed.), *Handbook of Hydrology*, (McGraw-Hill: New York), 5.1-5.51

Richards, K. 1993. Sediment delivery and the drainage network. In Beven, K. and Kirkby, M.J. (eds), *Channel Network Hydrology*, John Wiley & Sons, Chichester, p221-254.

Soil Conservation Service, 1972, *SCS National Engineering Handbook, Sec. 4, Hydrology*, USDA.

Thornes, J.B., 1985, The ecology of erosion, *Geography*, 70, 222-234.

Thornes, J.B., 1989, Erosional equilibria under grazing. *In* Bintliff, J., Davidson, D., and Grant, E. (eds), *Conceptual Issues in Environmental Archaeology*, (University Press: Edinburgh), 193-210.

Vandelannoote, A., Robbertson, H., Deelstra, H., Vyumvuhore, F., Bitetera, L. and Ollevier, F. (1996), The impact of the River Ntahangwa, the most polluted Burunidan affluent of Lake Tanganyika, on the water quality of the lake, *Hydrobiologica*, 328, 161-171.

Walling, D.E. 1983. The sediment delivery problem. *Journal of Hydrology*, **65**:209-237.

Walling, D.E. 1988. Erosion and sediment yield-some recent perspectives. *Journal of Hydrology*, **100**:113-141.

Zhang, X., Drake, N.A., Wainwright, J., and Mulligan, M. (Accepted 1998) Comparison of slope estimates from low resolution DEMs:Scaling issues and a fractal method for their solution, Earth Surface Processes and Landforms.

Zhang, X. Drake, N.A. Wainwright, J. and Mulligan, M., submitted, Comparison of GIS based models for estimating monthly land surface fluxes at the global scale.

8. Appendix 1. Scaling Vegetation Cover

To overcome the vegetation cover scaling problem it is necessary to consider the effects of variations in the fine scale spatial distribution of vegetation cover. To do this we have developed an approach that uses the frequency distribution of vegetation cover within a large pixel to describe the spatial variation of vegetation at a finer scale. We have taken this approach because to overcome the scaling problem we only need to know the variation in cover within a large pixel and not the spatial location of each patch of vegetation within the pixel.

To investigate the change in the frequency distribution of vegetation cover with scale, and to develop methods for predicting these changes, we developed a multi-scale database of vegetation cover images derived from ground measurements of cover using digital photography (approximately 1mm scale), and linear mixture modelling (Settle and Drake

1993) of digitised true colour aerial photography (0.55m), Landsat TM (30m) and NOAA-AVHRR (1.1 km) imagery in the Guadelintin Basin, southern Spain .

Analysis of this multi-scale data set showed that the histogram of the very high resolution vegetation cover images go through large but predictable changes as their spatial resolution is decreased (Figure A1a). Field measurements of vegetation cover are usually measured at the millimetre scale in the field (i.e. in the case of photographic methods of measuring cover, vegetation is recorded as being either present or absent at a chosen point in a photograph and then converted to a percentage). If all the points in the photograph are plotted as a histogram, then for 50% cover, the histogram will consist of two bars of equal height (Figure A1a). If the spatial resolution is reduced to a centimetre then the histogram will begin to form a U shape as a few pixels will begin to become mixed (Figure A1a). When the resolution is further reduced the histogram will form a bell shape in the case of 50% cover or a skewed distribution in the case of more or less cover. Such changes in histogram shape occur over all scales investigated by us and can be simulated using a Polya mass function to describe the general shape of the vegetation frequency distribution at a specified scale (Figure A1b). The Polya distribution is a mixture distribution of a beta and binomial distribution and is represented as:

$$f(x) = {}^{n}C_{x}\int_{0}^{1}\theta^{x}(1-\theta)^{n-x}\left[\Gamma(\alpha+\beta)/\Gamma(\alpha)\Gamma(\beta)\right]\theta^{\alpha-1}(1-\theta)^{\beta-1}d\theta \qquad (3)$$

$$= {}^{n}C_{x}\left[\Gamma(\alpha+\beta)/\Gamma(\alpha)\Gamma(\beta)\right]\int_{0}^{1}\theta^{x+\alpha-1}(1-\theta)^{n-x+\beta-1}d\theta \qquad 0 \le x \le n \le N \qquad (4)$$

where $\Gamma(\alpha) = \int_{0}^{\infty} x^{\alpha-1}e^{-x}dx$, ${}^{n}C_{x} = \dfrac{n!}{x!(n-x)!}$, n is the number of events, α and β are defined by the variance and mean, x is a random variable between 0 and n, and θ is a variable that ranges between 0 and1. Figure A1b shows that many different histograms can be simulated by changing the value of α and β.

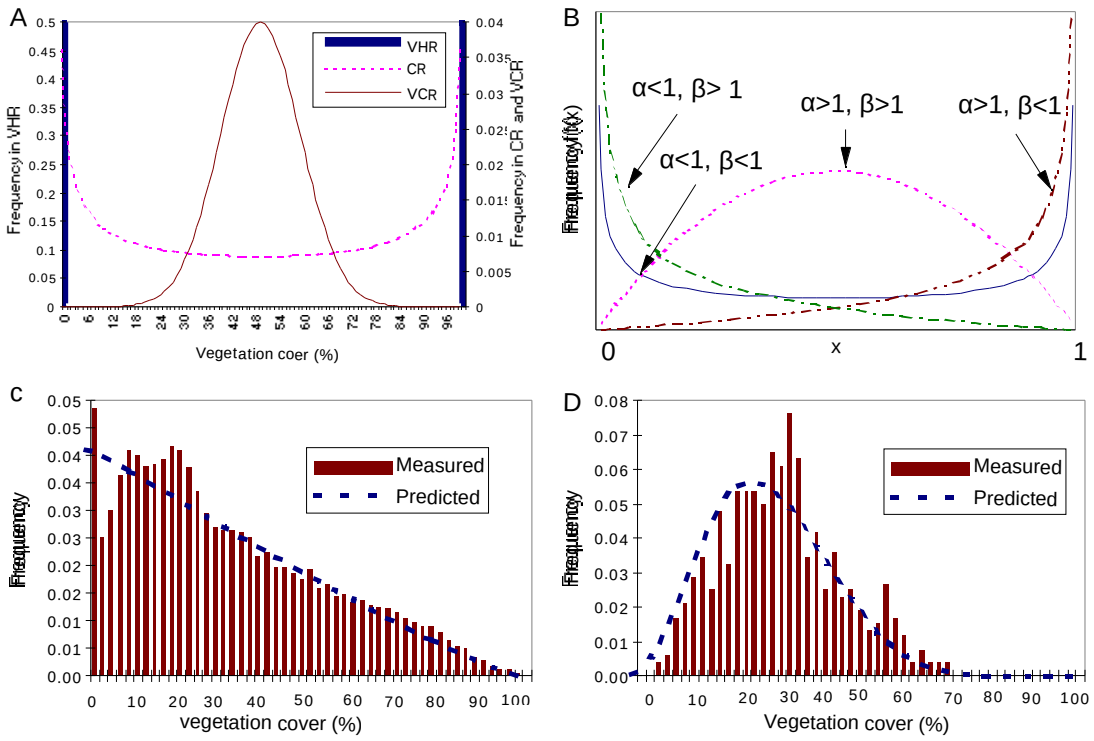

Figure A1. A) Change in the frequency distribution of vegetation cover from very high resolution (1mm) to a coarser resolution (CR) and a very coarse resolution. B) Examples of the histograms that can be simulated by the Poyla function using different values of α and β. C) Histograms of vegetation cover in an agricultural area and the frequency distributions predicted the Poyla function using a pixel size of 0.55 m, RMS= 0.0027B. D) Same as C but with a pixel size of 5.5 m, RMS=0.0046.

When the simulated distribution is compared with that measured from the 0.55m vegetation cover image (Figure A1c) the low RMS error indicates that the simulated frequency distribution is close to measured values at high cover, however, the fit is poor at low cover where there are two modes. When the image pixel size is enlarged 10 times the pixels with bare soil disappear and the frequency distribution of vegetation cover changes considerably and though the RMS is increased slightly the fit is still quite good (Figure A1b). By analysing the other images at coarser scales we have shown that the Polya mass function can successfully simulate the frequency distribution of numerous spatial distributions and scales of vegetation cover, however, peaks in the histogram at the extreme vegetation cover levels (0 and 100%) are never predicted very well.

The results of changing the spatial resolution show that though the mean is stable across scales the variance is reduced at increasingly coarser scales (Figure A2). Some means of predicting this reduction in variance is needed in order to calculate the Poyla function in order to predict the frequency distribution at the fine scales from coarse resolution data. We have found that the subimage variance, estimated by dividing the air photo vegetation cover image into 8x8 pixel subimages, shows a consistant pattern in variance reduction with increasing pixel size (Figure A2). The curve shapes in different subareas are a function of the resolution, and variance at a specified scale (d) can be predicted by $\sigma^2 = a + b \ln(d)$.

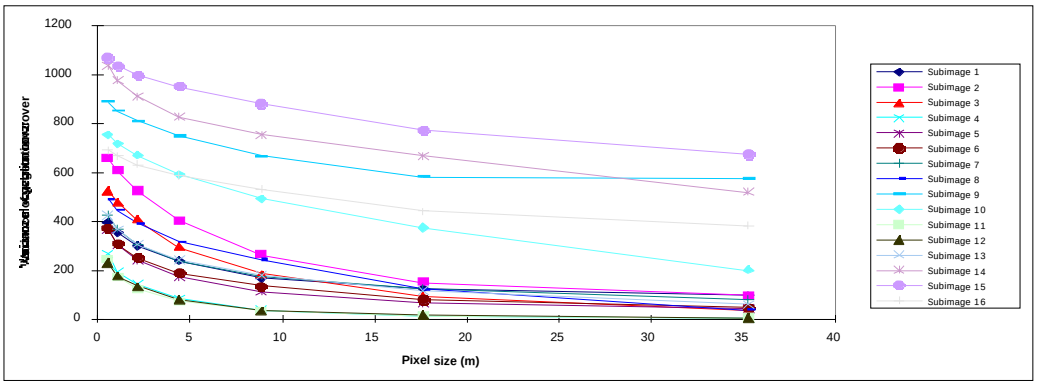

Figure A2. The relationship between subimage variance of vegetation cover and the spatial resolution of the subimages. The model $\sigma^2 = a + b \ln(d)$ (where and *a* and *b* are coefficients), fits this data well (mean r^2 = -0.989, maximum $r^{2=}$ -0.999, minimum $r^{2 =}$ -0.946) and allows prediction of the variance at a specified scale (*d*).

Thus subimage variance can be predicted across scales using a numerical model but this requires a reduction in spatial resolution so that *a* and *b* can be calculated for each subimage. We found that it is just about possible to estimate the variance at a specified scale *d* using a 5 x 5 subimage but the results using a 8 x 8 subimage are statistically better (Figure A3).

In order to test how the technique works at progressively coarser scales TM estimates of cover were validated using the air photos and the AVHRR validated using TM. The results of the comparison showed similar RMs errors to those outlined above, however, that large areas of bare soil cause problems at the TM and AVHRR scale as do histograms with multiple modes, though the fit is better at the AVHRR scale.

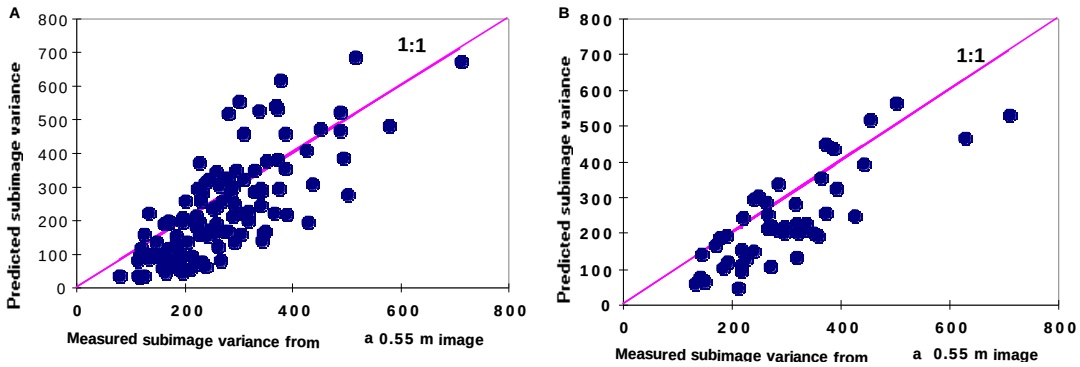

Figure A3. Variance within; A) a 5 by 5 subimage, and B) an 8 by 8 subimage estimated at 0.55 m resolution from a 17.63 m resolution image. The r^2 between the actual and predicted variances is 0.57 for the 5 by 5 kernel and 0.67 for the 8 by 8 kernel. The predicted values duplicate the measured values well though there is a slight underestimation of predicted variance.

9. Appendix 2 Sediment Yield Estimates Derived via the Soil Erosion & Routing Model

Table 1. Sediment transported to the Lake Tanganyika during March 1996 (Tonnes).

River No.	a	b	c	d	e	f	g	h	I	j
03/03/96	0.0	0.0	36.9	48.0	0.0	0.0	0.0	0.0	0.0	0.0
07/03/96	0.0	0.0	0.0	0.0	1651.3	0.0	154.0993	1986.7	39.0	85.4
09/03/96	0.0	0.0	0.0	0.0	25.0	0.0	0.502605	5.8	0.2	0.84
12/03/96	0.0	0.0	378.5	401.7	14226.7	811.3	1831.234	2201.2	0.0	0.0
13/03/96	0.0	0.0	1.0	0.0	5.6	0.0	0.004934	0.0	0.0	0.0
14/03/96	464.4	42.4	363.7	35.1	20203.0	182.4	2177.557	18253.9	174.7	68.6
18/03/96	0.0	0.0	0.0	0.0	0.0	0.0	0.0	0.0	0.0	0.0
19/03/96	0.0	0.0	0.0	0.0	0.0	0.0	0.0	0.0	0.1	0.5
20/03/96	0.0	0.0	262.9	7.5	12473.1	58.2	878.9552	9199.8	54.3	38.3
23/03/96	0.0	0.0	85.8	1.5	0.0	0.0	0.0	0.0	0.0	0.0
26/03/96	10.1	9.3	234.2	2.7	12691.8	40.0	217.0921	7349.0	1396.5	217.4
29/03/96	34.5	18.0	15.7	0.0	740.7	0.2	1.774035	137.1	0.3	1.0
30/03/96	3036.6	3878.8	14723.5	938.6	35822.3	151.1	518.7044	15261.0	2490.9	318.7
31/03/96	1660.3	568.1	557.1	54.4	4735.5	73.1	185.9948	394.7	0.51	0.4
Total	5206.0	4516.6	16659.2	1489.4	102575.3	1316.28	5965.919	54789.3	4156.4	731.2

River No.	k	l	m	n	o	p	q	r	s	t
03/03/96	0.0	0.0	0.0	0.0	0.0	0.0	0.0	0.0	0.0	0.0
07/03/96	923.1	1401.4	940.3	258963.2	181.0	162.5	507.6	89.0	51.4	503.3
09/03/96	9.3	14.5	9.1	5154.8	6.9	7.6	19.7	3.4	1.3	29.8
12/03/96	0.0	0.0	0.0	0.0	0.0	0.0	1.5	8.6	180.0	119.0
13/03/96	0.0	0.0	0.0	0.0	0.0	0.0	0.2	0.8	4.4	0.2
14/03/96	641.0	1535.9	715.8	106359	18.8	302.6	3324.0	3766.3	8878.9	585.5
18/03/96	0.0	0.0	0.0	19850.3	0.1	1.8	9.2	5.4	10.2	0.1
19/03/96	5.6	14.1	7.1	9132.7	0.1	4.0	38.4	90.6	156.9	0
20/03/96	401.3	1122.4	592.3	287305.3	15.0	168.2	1658.1	1862.3	4324.0	168.5
23/03/96	0.0	0.0	0.0	0.0	0.0	0.0	0.0	0.0	0.0	0.0
26/03/96	1175.5	1202.7	534.4	137434.9	329.7	732.2	749.7	77.1	104.5	2532.8
29/03/96	11.1	12.1	5.2	5601.6	5.5	14.3	13.6	0.2	1.7	81.9
30/03/96	1329.7	1204.4	514.8	186186.5	207.1	473.7	605.0	61.5	92.5	2443.9
31/03/96	4.8	3.0	0.5	7.9	0.4	1.9	2.3	0.0	1.7	393.9
Total	4501.4	6510.6	3319.5	1015996	764.5	1868.9	6929.2	5965.2	13807.5	6858.9

Table 1. (Continued).

River No.	u	v	w	x	y	z	1	2	3	4	5
03/03/96	0.0	0.0	0.0	0.0	120.6	59.1	43.9	3.2	23.9	59.8	0.0
07/03/96	446.8	0.5	0.1	0.0	0.0	0.0	0.0	0.0	0.0	0.0	0.0
09/03/96	24.8	0.2	0.3	0.0	0.0	0.0	0.0	0.0	0.0	0.0	0.0
12/03/96	111.2	17574.3	18941.7	5350.3	44323.2	6345.3	795.8	0.1	17.3	121.8	0.0
13/03/96	0.7	180.9	204.7	70.6	1152.1	282.8	160.3	0.1	165.3	299.1	0.0
14/03/96	761.5	5689.5	5477.0	878.0	10062.6	2046.7	424.4	0.3	237.2	242.9	0.0
18/03/96	0.9	0.0	0.0	0.0	0.0	0.0	0.0	0.0	0.0	0.0	0.0
19/03/96	0.	0.0	0.0	0.0	0.0	0.0	0.0	0.0	0.0	0.0	0.0
20/03/96	298.5	1840.6	1724.3	178.5	2204.2	553.1	59.1	0.0	40.8	48.7	0.0
23/03/96	0.0	0.0	0.0	0.0	3.2	1.3	0.4	0.0	0.0	0.2	0.0
26/03/96	14487.1	18971.0	6426.2	329.0	3360.8	1144.1	23.8	2.1	3.1	43.8	0.0
29/03/96	532.9	545.4	125.6	3.8	44.2	17.8	0.0	0.0	0.0	0.3	6.4
30/03/96	17912.3	30567.7	13472.6	1489.9	29571.3	11699.6	1099.3	1121.5	1824.6	8473.9	4454.5
31/03/96	2380.0	7531.8	4355.4	346.3	2330.7	685.4	22.2	0.9	1.3	10.4	0
Total	36957.5	82901.9	50727.9	8646.4	93172.9	22835.2	2629.1	1128.2	2313.5	9300.9	4460.9

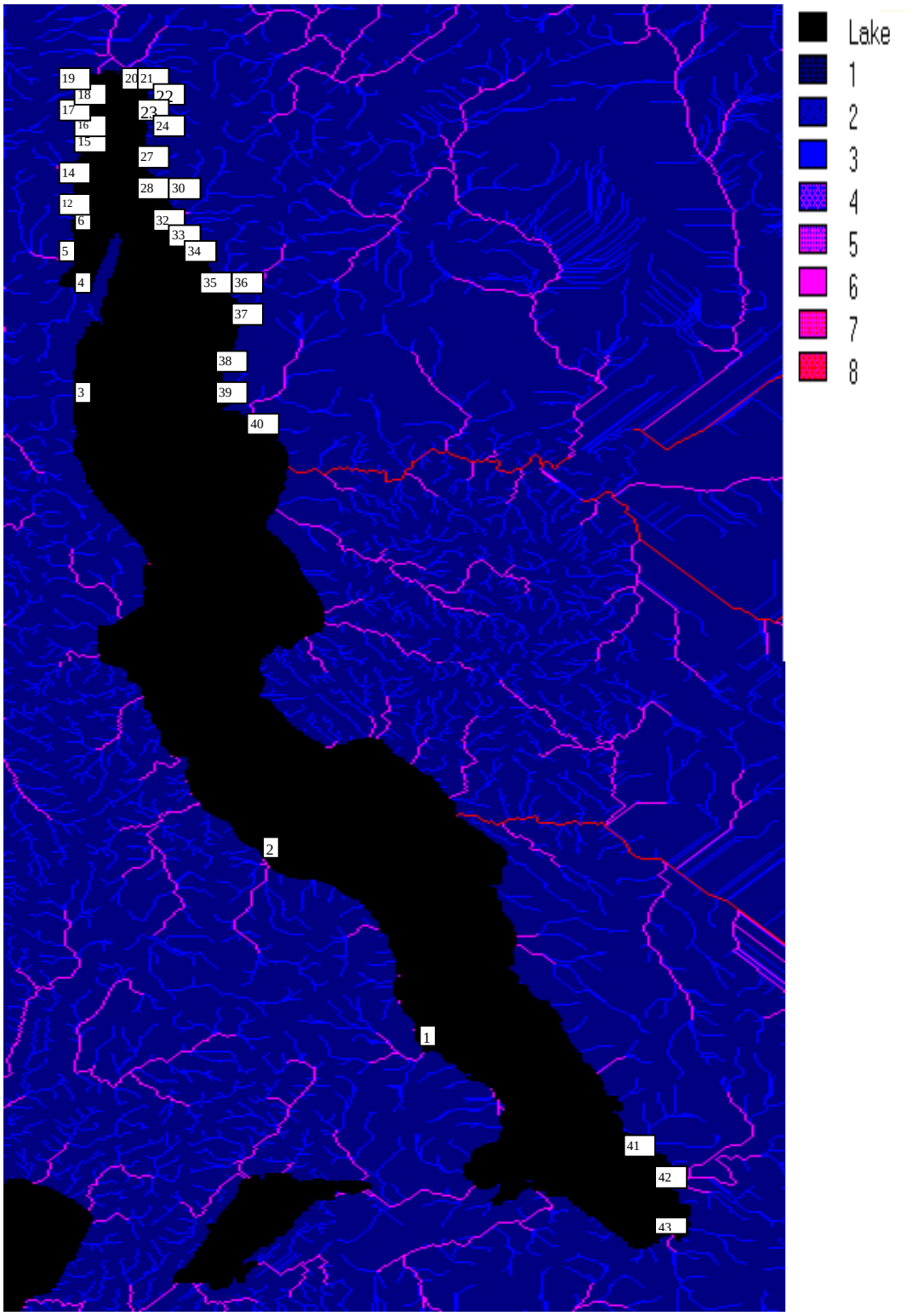

Figure A4. Channel network showing identifier numbers for the rivers that provided sediment into Lake Tanganyika in April 1998. See Table A2 for sediment yields.

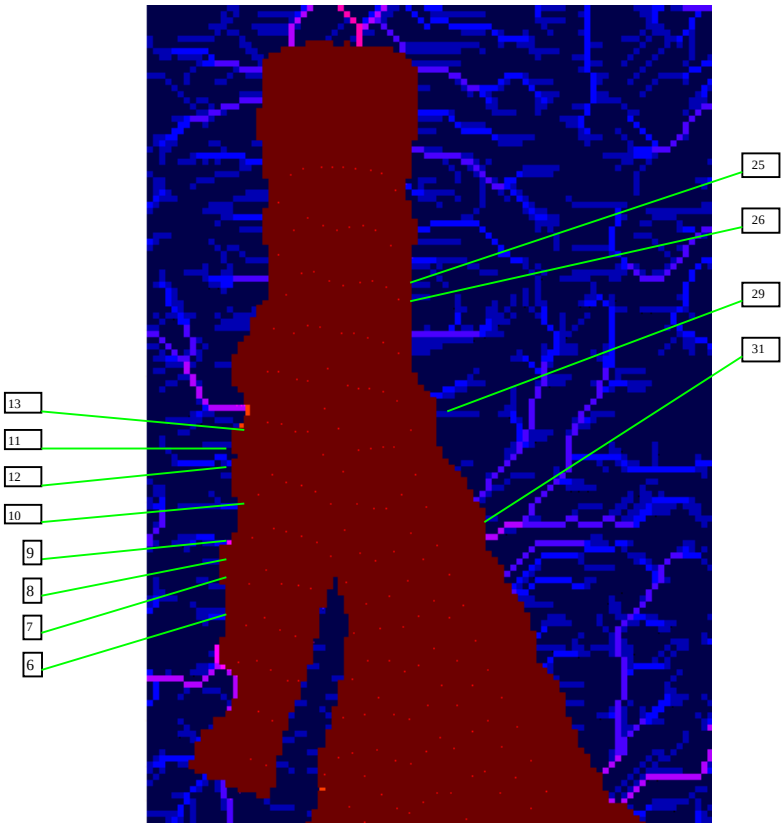

Figure A4. Continued.

River Identification Number	1	2	3	4	5	6	7	8
Catchment Area (km^2)	1573.5	334.8	163.4	418.6	1041.5	12.0	7.7	10.3
Sediment Delivery (tonnes)								
1st Dekad	42.0	4.4	0.0	8.9	3.6	0.0	0.0	0.2
2nd Dekad	104.3	3.8	10.2	295.2	3187.3	9.7	5.4	93.3
3rd Dekad	0.0	0.0	0.0	1.4	0.0	0.0	0.0	0.0
Total Sediment Yield (tonnes/km^2)	0.1	0.03	0.1	0.7	3.1	0.8	0.7	9.1
Catchment Sedimentation								
1st Dekad	107.7	10.9	0.0	21.5	8.6	0.0	0.0	0.4
2nd Dekad	268.2	9.6	24.7	704.7	7615.8	25.2	13.4	220.3
3rd Dekad	0.0	0.0	0.0	3.5	0.0	0.0	0.0	0.0
Total Sedimentation (tonnes/km^2)	0.2	0.1	0.2	1.7	7.3	2.1	1.8	21.5

River Identification Number	9	10	11	12	13	14
Catchment Area (km^2)	6.9	8.6	9.4	47.1	6.9	347.0
Sediment Delivery (tonnes)						
1st Dekad	0.2	0.1	0.1	0.0	0.0	14.5
2nd Dekad	96.2	54.4	54.5	132.9	249.3	4838.7
3rd Dekad	0.0	0.0	0.0	0.0	0.0	0.0
Total Sediment Yield (tonnes/km^2)	14.1	6.4	5.8	2.8	36.4	14.0
Catchment Sedimentation						
1st Dekad	0.5	0.3	0.4	0.0	0.1	36.7
2nd Dekad	222.9	131.2	137.3	316.6	549.1	12237.4
3rd Dekad	0	0	0	0	0	0.0
Total Sedimentation (tonnes/km^2)	32.6	15.4	14.6	6.7	80.1	35.4

River Identification Number	15	16	17	18	19	20	21
Catchment Area (km^2)	95.1	26.6	84.8	111.4	11.1	2571.12	132.0
Sediment Delivery (tonnes)							
1st Dekad	0.1	0.0	0.0	0.0	0.0	0.0	0.0
2nd Dekad	79.3	5.3	59.4	81.0	71.1	11030.7	151.4
3rd Dekad	0.0	0.0	0.0	0.0	0.0	0.0	0.0
Total Sediment Yield (tonnes/km^2)	0.8	0.2	0.7	0.7	6.4	4.3	1.2
Catchment Sedimentation							
1st Dekad	0.2	0.0	0.0	0.0	0.0	0.0	0.0
2nd Dekad	185.0	11.8	142.0	200.9	184.8	27067.9	368.3
3rd Dekad	0.0	0	0	0	0	0	0
Total Sedimentation (tonnes/km^2)	1.9	0.4	1.7	1.8	16.6	10.5	2.8

Table A2. Catchment Sedimentation and Sediment Transported to Lake Tanganyika in April 1998 (Tonnes).

River Identification Number	22	23	24	25	26	27	28	29
Catchment Area (km^2)	61.7	218.5	74.6	28.3	55.7	105.4	48.8	16.3
Sediment Delivery (tonnes)								
1st Dekad	0.0	1.7	0.9	0.0	0.3	0.1	3.4	0.7
2nd Dekad	78.2	831.0	314.0	33.2	91.1	142.2	422.1	79.0
3rd Dekad	0.0	0.0	0.1	0.0	0.0	0.0	0.0	0.0
Total Sediment Yield (tonnes/km^2)	1.3	3.8	4.2	1.2	1.6	1.4	8.7	4.9
Catchment Sedimentation								
1st Dekad	0.0	4.2	2.1	0.0	0.7	0.3	7.9	1.6
2nd Dekad	187.0	2032.9	779.9	83.0	214.4	336.4	1002.9	187.5
3rd Dekad	0.0	0.0	0.0	0.0	0.0	0.0	0.1	0.0
Total Sedimentation (tonnes/km^2)	3.0	9.3	10.5	2.9	3.9	3.2	20.7	11.6

River Identification Number	30	31	32	33	33	34	35	36
Catchment Area (km^2)	280.2	5.1	448.9	48.0	98.5	38.5	455.3	583.2
Sediment Delivery (tonnes)								
1st Dekad	40.2	1.7	145.4	5.0	49.1	15.3	21.5	11.3
2nd Dekad	1016.6	33.0	4507.6	307.1	1763.7	681.0	1360.4	1138.7
3rd Dekad	4.9	0.3	18.7	0.3	4.0	0.6	15.8	0.2
Total Sediment Yield (tonnes/km^2)	3.8	6.8	10.4	6.5	18.4	18.1	3.1	2.0
Catchment Sedimentation								
1st Dekad	99.8	4.0	364.0	15.6	131.4	36.1	52.1	26.5
2nd Dekad	2501.5	76.6	11218.4	859.6	4567.1	1606.9	3267.0	2705.0
3rd Dekad	12.1	0.6	46.7	1.1	10.9	1.5	1.6	0.5
Total Sedimentation (tonnes/km^2)	9.3	15.8	25.9	18.3	47.8	42.8	7.3	4.7

River Identification Number	37	38		39	40	41	42	43
Catchment Area (km^2)	72.8	6.0	6.8	171.1	2400.4	1018.7	2694.4	685.1
Sediment Delivery (tonnes)								
1st Dekad	174.3	0.0	0.0	0.0	11.5	0.0	44.7	509.5
2nd Dekad	7337.1	19.7	15.8	3.3	1467.6	5.5	36.3	166.2
3rd Dekad	8.8	0.0	0.0	0.0	0.2	0.0	0.0	0
Total Sediment Yield (tonnes/km^2)	103.3	3.3	2.3	0.0	0.6	0.0	0.0	1.0
Catchment Sedimentation								
1st Dekad	432.7	0.1	0.1	0.0	28.1	0.0	110.0	1291.1
2nd Dekad	18204.6	52.8	43.1	7.9	3646.8	12.5	90.0	418.4
3rd Dekad	21.8	0.0	0.0	0.0	0.5	0.0	0.0	0.0
Total Sedimentation (tonnes/km^2)	256.4	8.8	6.3	0.1	1.5	0.0	0.1	2.5

Table A2. continued.